



# Review on the Oxidation of Metallic Thermal Sprayed Coatings: A Case Study with Reference to Rare-Earth Permanent Magnetic Coatings

Jo Ann Gan and Christopher C. Berndt

(Submitted December 6, 2012; in revised form May 29, 2013)

Thermal spray fabrication of rare-earth permanent magnetic coatings (PMCs) presents potential manufacturing routes for micro-magnetic devices. Despite this potential, thermal spray of PMCs is still not widely explored due to oxidation concerns. It was established that oxidation leads to the loss of ferromagnetic phases in these materials and results in deterioration of magnetic performance. Although this review focuses on a specific class of material, i.e., magnetic materials, there is significant technical crossover to all classes of feedstocks that are employed in thermal spray processing. The oxidation mechanisms and the associated influencing factors are explored in this work to implement effective processing techniques during the deposition process. This paper reviews the various stages and mechanisms of oxidation in thermal spray processes. The factors that influence the extent of oxidation depend on the type of oxidation that is dominant and rely on the type of spray system, powder injection position, and the particle size of feedstock. Among the aspects that are reviewed include the oxygen-fuel ratio for high velocity oxygen-fuel (HVOF), current intensity, gas flow rate, particle size, spray distance, and substrate temperature. Protection strategies to minimize oxidation in thermal spray processes, such as gas shrouding and shielding, are presented.

**Keywords** in-flight oxidation, oxidation, oxidation protection, permanent magnet, post-impact oxidation, rare-earth, thermal spray coatings

## 1. Introduction

The oxidation of thermal spray coatings has become a subject of great interest because it influences the performance of coatings. Of great concern is the fact that oxidation deteriorates the functioning of thermal barrier coatings (TBCs) and other high temperature corrosion-resistant coatings. In TBCs, coatings are subjected to irregular degradation during thermal cycling due to the coefficient of thermal expansion mismatch between metal and oxides (Ref 1). Chemical uniformity of surfaces exposed to corrosion is disrupted by oxidation and hence depreciates the corrosion resistance capability (Ref 2). Coatings that are formed with oxides are also more brittle, which makes them difficult to machine for certain applications since the mechanical properties of the coatings are

affected. Also, spalling of coatings has become a common phenomenon in the presence of oxides.

However, a certain degree of oxidation is desirable in several applications. It has been demonstrated that oxides improve the wear resistance of a coating (Ref 3) and increase the coating hardness. The strength of a coating under compressive loading is also enhanced in the presence of oxides (Ref 4, 5). Metal oxides that reside along the splat boundaries can alter the intersplat cohesion, while oxide dispersion in the splat itself or supersaturated oxygen strengthens the splat (Ref 4, 6).

Most of the studies on oxidation of thermal spray coatings were conducted using steel or steel alloys because steels are (i) sensitive to oxidation and (ii) widely used as corrosion and wear-resistant coatings. The study on thermal sprayed permanent magnetic coatings (PMCs) has been limited due to the lack of understanding in the oxidation behavior of the permanent magnets, especially for rare-earth magnets.

Rare-earth transition-metal magnets exhibit the strongest magnetic behavior among all the other hard magnetic materials, such as alnico and ceramic magnets. Neodymium iron boron and samarium cobalt are the two most commonly used rare-earth hard magnets that demonstrate high overall magnetic performance. Neodymium iron boron is the stronger among the two, having bulk remanence, coercivity, and maximum energy product in the range of 1.0–1.4 T, 9.5–25 kOe, and 25–55 MGOe, respectively. Rare-earth permanent magnets are widely used in many industries, from aerospace and automotive to

Jo Ann Gan and Christopher C. Berndt, Industrial Research Institute Swinburne, Faculty of Engineering and Industrial Sciences, Swinburne University of Technology, Hawthorn, VIC 3122, Australia; and Christopher C. Berndt, Department of Materials Science and Engineering, Stony Brook University, Stony Brook, NY 11794. Contact e-mail: jgan@swin.edu.au.

telecommunication and electronic devices (Ref 7). Thick films or coatings of these materials can be applied in microelectromechanical systems (MEMS) (Ref 8, 9) for applications such as micro-actuators, micro-motors, and micro-generators. One downfall of the rare-earth magnet, however, is the strong affinity of rare-earth elements to oxygen, which makes them prone to oxidation during processing and operation.

Oxidation leads to brittle coatings and deterioration of magnetic properties. However, studies to find alternatives to control the oxidation process have been limited. Most studies on the fabrication of permanent magnet films have focused on low temperature processes such as sputtering: a thin film method that has technical limitations with regard to processing time, restrictions concerning the geometry and size of the component, and a cost penalty. In cases where thermal spray has been employed, spraying has been mostly performed within a vacuum chamber to minimize oxidation (Ref 10-12). Recent studies have examined the low temperature cold spray process (Ref 13). Although the coating obtained did not exhibit oxidation or deterioration of magnetic properties, the coating was too brittle to be of practical use.

Whether oxidation is desired or otherwise, the ability to control the degree of oxidation in a coating is important for the coating to achieve optimum performance. The mechanism of oxidation must be understood to manipulate the oxidation process to advantage. This paper is devoted to reviewing the oxidation considerations in depositing PMCs. The stages and mechanisms of oxidation in the thermal spray process, factors that influence oxidation, and protection measures against oxidation during thermal spray processing are investigated. The thermal oxidation of rare-earth permanent magnets is highlighted since they are prone to high temperature oxidation and a prime reason regarding the poor acceptance on depositing magnetic coatings *via* thermal spray.

## 2. Oxidation of Permanent Magnetic Coatings

Oxidation has been a concern for thermal spray PMCs. PMCs are conventionally fabricated by lower temperature processing methods such as sputtering (Ref 14, 15), screen printing (Ref 16, 17), and tape casting (Ref 18, 19). The research on thermal spray PMCs has been confined to the use of vacuum plasma spray (Ref 10, 11, 20) and cold spray (Ref 13). Much research has examined the oxidation of PMCs throughout the aging process, but few have studied oxidation during the fabrication process. Therefore, the understanding of PMC oxidation is limited. The PMCs in this section refer to rare-earth transition metals, specifically neodymium iron boron ( $\text{Nd}_2\text{Fe}_{14}\text{B}$ ) and samarium cobalt ( $\text{SmCO}_5$  and  $\text{Sm}_2\text{CO}_{17}$ ), since they are more prone to oxidation than magnetoplumbite-type ferrites, which are already in an oxidized state.

Earlier studies indicated that oxidation products of different phases depended on temperature and humidity

(Ref 21, 22). Generally, corrosion of rare-earth magnets can occur under three conditions: (i) warm humid air or steam (Ref 23-25), (ii) electrochemical reactions (Ref 26-28), and (iii) exposure to high temperature ( $>250^\circ\text{C}$ ) for long time periods (from several hours up to days) (Ref 29, 30). Of these three adverse conditions, permanent magnet particles are most prone to be subjected to high temperature oxidation during thermal spray. Although the thermal spray process involves very short processing time [between 0.1 and a few milliseconds (Ref 31, 32)], oxidation still occurred due to the high temperature involved in thermal spray processes (Ref 10, 33, 34). Therefore, the oxidation product of thermal spray permanent magnets was similar to those of bulk magnets. A prime difference would be that the oxidation process of thermal spray permanent magnets occurred at a much higher rate and any intermediate oxidation products might not be observed.

The oxidation of neodymium iron boron and samarium cobalt is a two-stage process: (i) formation of external scales and (ii) internal oxidation (Ref 35, 36). The external scales are free of rare-earth elements and consist of  $\text{Co}_3\text{O}_4$  and  $\text{CoFe}_2\text{O}_4$  for samarium cobalt (Ref 37), and  $\alpha\text{-Fe}_2\text{O}_3$  (hematite) accompanied by  $\text{Fe}_3\text{O}_4$  (magnetite) for neodymium iron boron (Ref 36). Internal oxidation can be prevented if the external oxide layers can restrict the access of oxygen. However, these oxide layers are not protective at elevated temperatures (Ref 36) and result in an internal oxidation zone (IOZ). Internal oxidation is the primary degradation mechanism for rare-earth transition-metal materials and is more detrimental than external oxides since the IOZ is much thicker than the surface oxides and phase transformations in this region destroy the hard magnetic properties of the alloy (Ref 36-38). The IOZ in samarium cobalt is composed of  $\alpha\text{-Co}$ ,  $\text{Sm}_2\text{O}_3$ , and  $\text{SmCoO}_3$  (Ref 35, 39), while the IOZ in neodymium iron boron is constituted of  $\alpha\text{-Fe}$ ,  $\text{Nd}_2\text{O}_3$ ,  $\text{NdFeO}_3$ , and  $\text{B}_2\text{O}_3$  (Ref 29, 36, 40). The structure of IOZ in samarium cobalt was described as parallel samarium oxide platelets and fibers surrounded by cobalt (Ref 41), whereas the IOZ structure of neodymium iron boron was described as neodymium oxide particles embedded in an  $\alpha\text{-Fe}$  matrix (Ref 36). Schematics of the IOZ of neodymium iron boron and samarium cobalt are shown in Fig. 1.

Since oxidation at elevated temperature is the primary cause for IOZ formation that is detrimental to the material properties compared to external oxides, the following sections are focused on thermal oxidation of neodymium iron boron and samarium cobalt. However, it should be noted that the oxidation mechanisms discussed in this section concern solid phase oxidation, while oxidation in thermal spray processes involves both solid and liquid phase oxidation. Solid phase oxidation represents the closest approximation of oxidation reactions at a high temperature available in the literature since there have been no reports in the open literature on liquid phase oxidation for these materials. Most studies for these materials were carried out to investigate oxidation during the materials' performance as a magnet rather than during processing or deposition. The significance of this section is

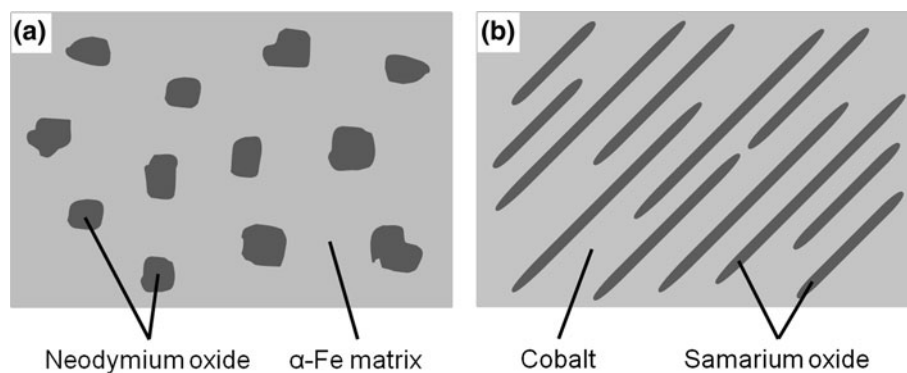
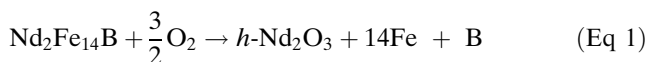


**Fig. 1** Schematics of the IOZ of (a) neodymium iron boron and (b) samarium cobalt

that it presents an overview of the potential oxidation mechanisms for rare-earth magnetic materials in thermal spray processing and phases that will be present in the coatings.

## 2.1 Neodymium Iron Boron (Nd-Fe-B)

The thermal oxidation of Nd-Fe-B occurs through the process of dissociation followed by oxidation. The  $\text{Nd}_2\text{Fe}_{14}\text{B}$  matrix dissociates into  $\alpha\text{-Fe}$  nanocrystals that consist of small hexagonal neodymium oxide,  $h\text{-Nd}_2\text{O}_3$ , precipitates and form a gray surface layer that grows transgranularly into the magnet. Further oxidation led to the formation of  $\alpha\text{-Fe}_2\text{O}_3$  and at approximately  $600\text{ }^\circ\text{C}$ , the  $\alpha\text{-Fe}_2\text{O}_3$  reacted with the small precipitates of  $h\text{-Nd}_2\text{O}_3$  formed earlier to give  $\text{NdFeO}_3$ . Another form of neodymium oxide exists in cubic structure,  $c\text{-Nd}_2\text{O}_3$ , which results from the oxidation of  $\text{NdO}_x$  (Nd-rich intergranular regions) (Ref 40). The reactions were proposed to occur according to Eq 1-4. The results of Li et al. (Ref 36) agreed with those of Edgley et al. (Ref 40). The proposed overall reaction for the oxidation of Nd-Fe-B varies throughout the literature and they are summarized in Table 1. Despite the variation in the proposed overall equation, the literature agrees on the same oxidation products, i.e.,  $\alpha\text{-Fe}$ ,  $\text{Fe}_2\text{O}_3$ ,  $\text{Fe}_3\text{O}_4$ ,  $\text{Nd}_2\text{O}_3$ , and  $\text{NdFeO}_3$ , although some of these oxidation products were not reflected in the overall equations.



Two types of  $\text{Nd}_2\text{O}_3$  were observed by Edgley et al. (Ref 40), namely, cubic and hexagonal  $\text{Nd}_2\text{O}_3$ . The cubic structure,  $c\text{-Nd}_2\text{O}_3$ , formed at lower temperature ( $<275\text{ }^\circ\text{C}$ ), while hexagonal,  $h\text{-Nd}_2\text{O}_3$ , was observed at  $240\text{-}350\text{ }^\circ\text{C}$ . In between  $240$  and  $275\text{ }^\circ\text{C}$ , both cubic and hexagonal  $\text{Nd}_2\text{O}_3$  coexisted. Another Nd-Fe-B phase that

was present other than  $\text{Nd}_2\text{Fe}_{14}\text{B}$  would be sub-stoichiometric  $\text{Nd}_{1.1}\text{Fe}_4\text{B}_4$  (Ref 29, 36, 40). However, the oxidation of this phase occurred at a higher temperature ( $>611\text{ }^\circ\text{C}$ ) and this has not been investigated further. The oxidation of  $\text{Nd}_{1.1}\text{Fe}_4\text{B}_4$  is noteworthy since it has potential significance with regard to the oxidation of thermal spray PMCs. Therefore, there are generally three main phases observed in Nd-Fe-B magnets: (i)  $\text{Nd}_2\text{Fe}_{14}\text{B}$ , (ii) Nd-rich ( $\text{NdO}_x$ ), and (iii)  $\text{Nd}_{1.1}\text{Fe}_4\text{B}_4$  (Ref 36, 42). Table 2 outlines the oxidation products for these three phases at temperatures below and above  $500\text{ }^\circ\text{C}$ . Note that the temperature discussed here is much lower than the operating temperature of thermal spray processes, where the deposition mechanism involves particle melting and rapid solidification.

Castaldi et al. (Ref 43) and others (Ref 44, 45) mentioned the formation of  $\alpha\text{-Fe}$  as a result of  $\text{Nd}_2\text{Fe}_{14}\text{B}$  oxidation at process temperatures between  $600$  and  $800\text{ }^\circ\text{C}$ . Other oxidation phases were not discussed in detail. Lileev et al. (Ref 45) found that there was as much as  $18\text{ wt.}\%$  Nd-O present in a Nd-Fe-B film sputtered in an inert atmosphere. The presence of Nd-O in sputtered Nd-Fe-B was explained by Chen et al. (Ref 46) as a result of one of the following mechanisms:

- The base pressure of the chamber was too high.
- The films were deposited at high temperatures so that more oxygen was degassed from the chamber system.
- The target of Nd-Fe-B alloy contained a large proportion of neodymium that was readily oxidized.

## 2.2 Samarium Cobalt (Sm-Co)

Studies concerning the oxidation of samarium cobalt are relatively scarce and are not fully explained. Most of the studies focused on the oxidation products and kinetics and little attention have been given to the mechanism of its thermal oxidation. The oxidation of samarium cobalt has received less attention than neodymium iron boron since samarium cobalt demonstrated a higher Curie temperature, i.e., the temperature above which a ferromagnetic material becomes paramagnetic, than neodymium iron boron (Ref 47). However, samarium cobalt is still

**Table 1 Proposed overall oxidation reactions for Nd-Fe-B from the literature**

Proposed overall reaction	Reference
$3\text{Nd}_2\text{Fe}_{14}\text{B} + 23\text{O}_2 \rightarrow 6\text{NdFeO}_3 + 10\text{Fe}_3\text{O}_4 + 3\text{Fe}_2\text{B}^a$	Turek et al. (Ref 52)
$\text{Nd}_2\text{Fe}_{14}\text{B} + 3\text{O}_2 \rightarrow 13\alpha\text{-Fe} + c\text{-Nd}_2\text{O}_3 + \text{FeBO}_3$	Edgley et al. (Ref 40)
$\text{Nd}_2\text{Fe}_{14}\text{B} + 3/2\text{O}_2 \rightarrow 14\alpha\text{-Fe} + c\text{-Nd}_2\text{O}_3$ (+ interstitial B)	
$\text{Nd}_2\text{Fe}_{14}\text{B} + 3/2\text{O}_2 \rightarrow 14\alpha\text{-Fe} + h\text{-Nd}_2\text{O}_3$ (+ interstitial B)	
$4\text{Nd}_2\text{Fe}_{14}\text{B} + 9\text{O}_2 \rightarrow 4\text{Nd}_2\text{O}_3 + 2\text{B}_2\text{O}_3 + 56\text{Fe}$	Li et al. (Ref 36)

<sup>a</sup> The overall equation provided in the original literature was not balanced.

The balanced equation should have 29 O<sub>2</sub> on the left-hand side rather than the stated 23 O<sub>2</sub>.

**Table 2 Oxidation reactions for Nd<sub>2</sub>Fe<sub>14</sub>B, Nd-rich, and Nd<sub>1.1</sub>Fe<sub>4</sub>B<sub>4</sub> phases at temperatures below and above 500 °C (Ref 40)**

<i>T</i> < 500 °C	<i>T</i> > 500 °C
$\text{Nd}_2\text{Fe}_{14}\text{B} \rightarrow \alpha\text{-Fe} \rightarrow \text{Fe}_2\text{O}_3$	$\text{Nd}_2\text{Fe}_{14}\text{B} \rightarrow \alpha\text{-Fe} \rightarrow \text{Fe}_2\text{O}_3$
$\text{Nd}_2\text{Fe}_{14}\text{B} \rightarrow \text{Nd}_2\text{O}_3 \rightarrow \text{Nd}_2\text{O}_3$	$\text{Nd}_2\text{Fe}_{14}\text{B} \rightarrow \text{Nd}_2\text{O}_3 \rightarrow \text{NdFeO}_3$
$\text{Nd-rich}(\text{NdO}_x) \rightarrow c\text{-Nd}_2\text{O}_3 \rightarrow c\text{-Nd}_2\text{O}_3$	$\text{Nd-rich}(\text{NdO}_x) \rightarrow \text{NdO}_x \rightarrow c\text{-Nd}_2\text{O}_3$
$\text{Nd}_{1.1}\text{Fe}_4\text{B}_4 \rightarrow \text{Nd}_{1.1}\text{Fe}_4\text{B}_4 \rightarrow \text{Nd}_{1.1}\text{Fe}_4\text{B}_4$	$\text{Nd}_{1.1}\text{Fe}_4\text{B}_4 \rightarrow \text{Nd}_{1.1}\text{Fe}_4\text{B}_4 \rightarrow \text{Unknown}$

subjected to oxidation since rare-earths are prone to oxidation, and the oxidation of magnetic particles is more critical than for bulk sintered magnets (Ref 48).

The primary oxidation product of samarium cobalt is Sm<sub>2</sub>O<sub>3</sub> (Ref 39, 41). Bartlett and Jorgensen (Ref 41) reported that thermal oxidation of SmCo<sub>5</sub> resulted in the formation of monoclinic sesquioxide Sm<sub>2</sub>O<sub>3</sub> at all temperatures, along with the polymorph of hexagonal α-Co and cubic β-Co. Another study by Yang et al. (Ref 39) reported that thermal oxidation of samarium cobalt commenced at 500 °C, where consumption of samarium by oxidation resulted in the transformation of rhombohedral Sm<sub>2</sub>Co<sub>17</sub> and hexagonal SmCo<sub>5</sub> into the body-centered cubic (bcc) Fe(Co) solid solution and face-centered cubic (fcc) Co(Fe), respectively. In other words, the Fe(Co) phase is the degraded magnetic phase of Sm<sub>2</sub>Co<sub>17</sub>, while Co(Fe) is the degraded magnetic phase of SmCo<sub>5</sub>. While several researchers (Ref 35, 39, 48–50) agreed with Bartlett and Jorgensen (Ref 41) on the formation of Sm<sub>2</sub>O<sub>3</sub> due to oxidation, Yang et al. (Ref 39) discovered another oxide phase, SmFeO<sub>3</sub>, in addition to Sm<sub>2</sub>O<sub>3</sub>. The proposed overall oxidation reaction of samarium cobalt also varies throughout the literature and these reactions are summarized in Table 3.

Although the oxidation products of bulk magnets found in these studies have been observed in thermal spray PMCs (Ref 10, 51), all these studies involved a lower temperature range in relation to the process temperature of thermal spray. There is a need for the oxidation process and products at higher temperature to be explored further if thermal spray of PMCs is to be implemented widely, since these oxidation products influence the magnetic and mechanical properties of the PMCs significantly. Oxidation of neodymium iron boron and samarium cobalt resulted in the loss of ferromagnetic phases to form paramagnetic oxides (Ref 42, 52), thus leading to a detrimental loss of coercivity (Ref 53, 54). For instance, Matsuura et al. (Ref 55) found that the coercivity of a Nd-Fe-B thin film (100 nm) decreased by 60% after oxidation.

The deterioration of magnetic properties as a consequence of oxidation is a collective action of (i) superposition of soft and hard magnetic phases, (ii) oxidation of surface layers, and (iii) spin reorientation that changes the magnetic *c*-axis structure (Ref 56). Dickens and Mazany (Ref 57) determined that there is a direct correlation between weight gain from oxidation and magnetic properties' deterioration, where a weight gain of 4.5% for Nd-Fe-B causes total magnetic loss since neodymium in all phases has been totally oxidized at this point. However, this study did not take into consideration the weight gain from other oxidation products such as Fe<sub>2</sub>O<sub>3</sub> and B<sub>2</sub>O<sub>3</sub>. While the oxide phases may be helpful for the growth of a *c*-axis texture of Nd<sub>2</sub>Fe<sub>14</sub>B grains during deposition, its presence during post-deposition annealing deteriorated the magnetic properties (Ref 46). These results suggest that some oxidation protection must be implemented during the deposition process of PMCs to preserve their magnetic properties.

### 3. Stages and Mechanism of Oxidation in Thermal Spray Process

#### 3.1 In-Flight and Post-Impact Oxidation

Many researchers have examined the stages of oxidation in thermal spray processes. There have been numerous models of coating oxidation and there are many similarities among these models. In general, oxidation occurred in two stages: (i) in-flight oxidation and (ii) post-impact oxidation.

Hackett and Settles (Ref 58) suggested that the HVOF flow field could be divided into three regions, Fig. 2, and therefore oxidation occurred at three stages. This idea was reinforced by Dobler et al. (Ref 59). Region I encompassed the point of particle injection within the nozzle up to the end of the visible plume, also termed as the jet core. In this area, particles were subjected to oxidation by the

**Table 3 Proposed overall oxidation reaction of Sm-Co from the literature**

Proposed overall reaction	Reference
$\text{SmCo}_5 + 3/4\text{O}_2 \rightarrow 1/2\text{Sm}_2\text{O}_3 + 5\text{Co}$	41
$4\text{Sm}_2\text{Co}_{17} + 57\text{O}_2 \rightarrow 4\text{Sm}_2\text{O}_3 + 34\text{Co}_2\text{O}_3$	49
$\text{Sm}_2\text{Co}_{17} + 3/2\text{O}_2 \rightarrow 17\text{Co} + \text{Sm}_2\text{O}_3$	50

free oxygen in the products of combustion in HVOF. Although the amount of free oxygen in this zone could be controlled by selecting the oxygen/fuel ratio of the combustion parameters, the flame still contained different oxidizing combustion products and the particle oxidation cannot be completely avoided. Spray particle dwell time in Region I was very short, approximately one millisecond, and the particle temperatures were relatively high.

Region II referred to the domain where the local atmosphere was entrained to the centreline of the flame, toward the end of the jet core, until the particle impinged onto the substrate. In-flight oxidation may have occurred in this region because the surrounding atmosphere consisted of up to 20% oxygen. The particle residence time in this region was also short, while the particle temperature was slightly lower than Region I due to the cooling effect of the entrained air. Although the particle residence time also depends on other parameters, such as the particle size distribution, gas flow rate, and injection position, the particle residence times in Region I and II were still within the order of milliseconds (Ref 31, 60).

Lastly, Region III specified the splat formed on the substrate immediately after impact and just before the next layer of splats was deposited. The exposure time was approximately ten times longer than the particle flight time. The initial splat temperature was high due to (i) transformation of kinetic energy of the particles into thermal energy and (ii) exposure to the flame. However, the splats cooled rapidly since the substrate temperature was comparatively low. Seventy-five percent of total oxidation takes place in either Region II or III (Ref 58). Table 4 summarizes the conditions that affect the oxidation process at respective regions.

Vardelle et al. (Ref 61) revealed that oxidation in a plasma spray process also occurred over three stages: (i) gas-solid phase oxidation during initial preheating of particles to their melting point, (ii) gas-liquid oxidation of the molten particles in-flight, and (iii) gas-solid oxidation of the splats after deposition and before the formation of subsequent splat layers. These three stages of oxidation also occur during the HVOF process. Zhang et al. (Ref 62) established that most oxidation occurs in the liquid phase, while the particle temperature and velocity have no significant effect on the thickness of the surface oxide layer ( $\sim 0.1 \mu\text{m}$ ) before particle melting.

On the other hand, Volenik et al. (Ref 63) classified oxidation processes according to stages in the plasma spray process, i.e., (i) the in-flight stage and (ii) the deposition, solidification, and cooling stages. In the first stage, powder was injected into the plasma plume and melted. The molten particles then interacted with the

plasma gas that has been altered by the entrainment of surrounding atmosphere. The first stage was usually very short (several milliseconds), but the reaction temperature was high. The second stage of oxidation involved the interaction of solidified deposits with a gaseous mixture that consisted mainly of the ambient atmosphere. This stage was typically much longer (several seconds or longer) than the first stage and the temperature decreased gradually. As can be seen, Volenik's model was similar to that of Hackett and Settles (Ref 58) where the first stage was equivalent to Region I and II in Hackett and Settles' model, while the second stage corresponded to Region III.

There are distinct similarities and differences in the oxidation stages between HVOF and plasma spray. Both processes involve the two main stages of oxidation mentioned earlier in this section, i.e., in-flight and post-impact oxidation. There are two regions where in-flight oxidation occurs in both processes: (i) a visible plasma plume or jet core consisting of the plasma gas or combustion gases, where the particles are injected, and (ii) a turbulent flow region where surrounding atmosphere is entrained into the system. While region (i) in the plasma spray process is oxygen free, the same region in HVOF could be oxidizing or reducing depending on the oxygen-to-fuel (O/F) ratio. The length of each region in plasma spray depends on the type of plasma gas and flow rates, current intensity, and torch design, while the combustion gas flow rates, O/F ratio, and torch design determine this factor in HVOF systems. Post-impact oxidation for both processes is the same since this stage depends on the interaction between the deposited splat and the surrounding atmosphere. This mechanism is essentially the same for both processes unless a vacuum or controlled atmosphere environment is used for either process.

### 3.2 Mechanisms of Oxidation

A detailed mechanism and schematic models of oxidation during the thermal spray process was presented by Deshpande et al. (Ref 2), where oxidation may take place in-flight, at the splat surface, and/or between passes. In-flight oxidation depended strongly on the amount of entrained air, the particle temperature, and the nature and turbulence of the flame. In-flight particles oxidation in the jet core and in the plume was controlled by a different mechanism, as pointed out by Syed et al. (Ref 64, 65).

Sobolev et al. (Ref 66) mentioned that there were two mass transfer processes that occurred during the interaction of liquid particles and oxygen. The mass transfer processes were the development of oxides due to chemical reactions between the surface of the liquid phase and oxygen as well as the diffusion of oxygen in the liquid. However, later studies found that the amount of oxides present was too high to be explained by diffusion models (Ref 67).

In the jet core, particles were melted and the liquid phase reacted with oxygen present in the combustion products and entrained air. For instance, low carbon steel particles were melted in HVOF (Ref 68) and plasma spray (Ref 69), and oxidized to form FeO, Fe<sub>2</sub>O<sub>3</sub>, and Fe<sub>3</sub>O<sub>4</sub>. At this stage, the motion of the liquid was induced by

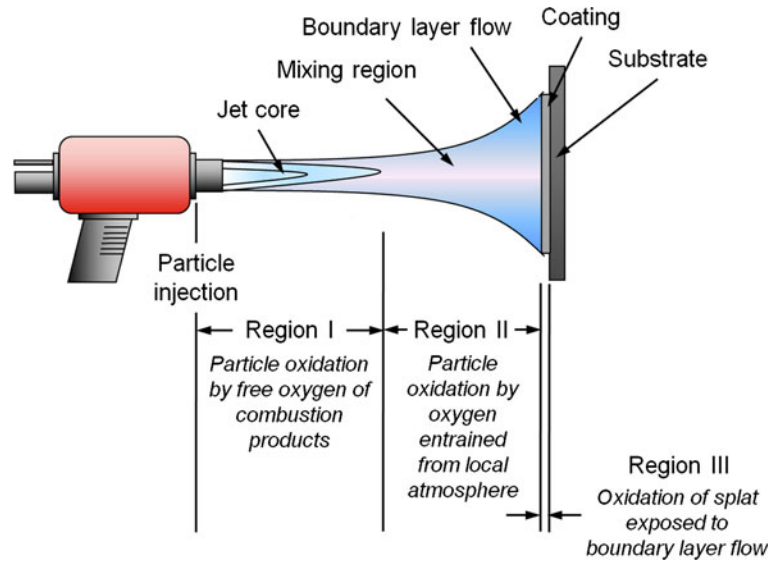


**Fig. 2** Schematic of the potential oxidation regions within a generic thermal spray process

**Table 4** Conditions affecting coating oxidation in Regions I, II, and III in HVOF jet (Ref 58)

	Region I	Region II	Region III
Estimated fraction of oxygen (%)	~2	~20	~20
Exposure time (s)	0.001	0.001	0.01-0.02
Relative temperature	High	Medium	High, then low
Particle shape	Sphere	Sphere	Splat

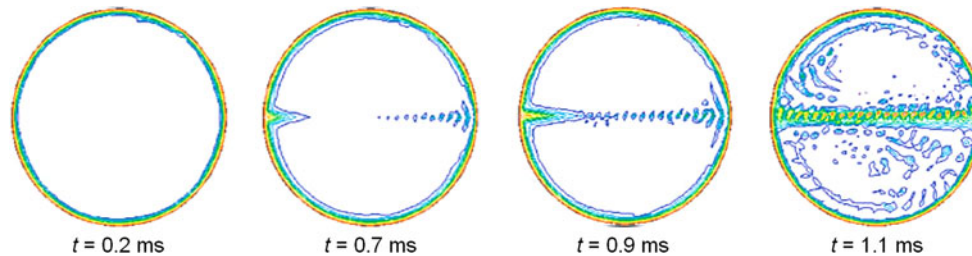


**Fig. 3** A model of convective movement by the spherical Hill vortex mechanism within an iron particle in the core of an Ar-H<sub>2</sub> plasma (Adapted from Ref 91)

convective movements, forming a spherical Hill vortex that resulted from the difference of kinematic viscosities between the liquid droplet and surrounding media (Ref 70). The spherical Hill vortex is a model that describes fluid motion or vortex distribution within a sphere (Ref 71). A model of oxide penetration by convective movement within an iron particle is depicted in Fig. 3. The generated vortex destroyed the surface oxides and distributed them uniformly through the bulk volume of the particle, forming nodular oxides, Fig. 4(a). The oxides were hurtled into the interior of the particle, leaving fresh metal on the particle surface, which enhanced the particle reactivity. The difference in surface tension between the

liquid oxides and metal encouraged the formation of isolated spherical nodules of oxide within the metal (Ref 69, 70), Fig. 5(b) and 6(a).

Outside the jet core, the velocities and temperatures of the plasma and particles converged, thus bringing down the Reynolds number ( $Re = \rho v D / \mu$  where  $\rho$ ,  $v$ ,  $D$ , and  $\mu$  are the density, velocity, diameter, and viscosity of the fluid, respectively) from over 25 at spray distance 35 mm to about 7.5 at 75 mm (Ref 69). As the kinematic viscosity decreased rapidly, the convective movement and oxide mass transfer from particle to surface also ceased. Therefore, formation of nodules only occurred within the first 40-50 mm downstream of the nozzle exit under

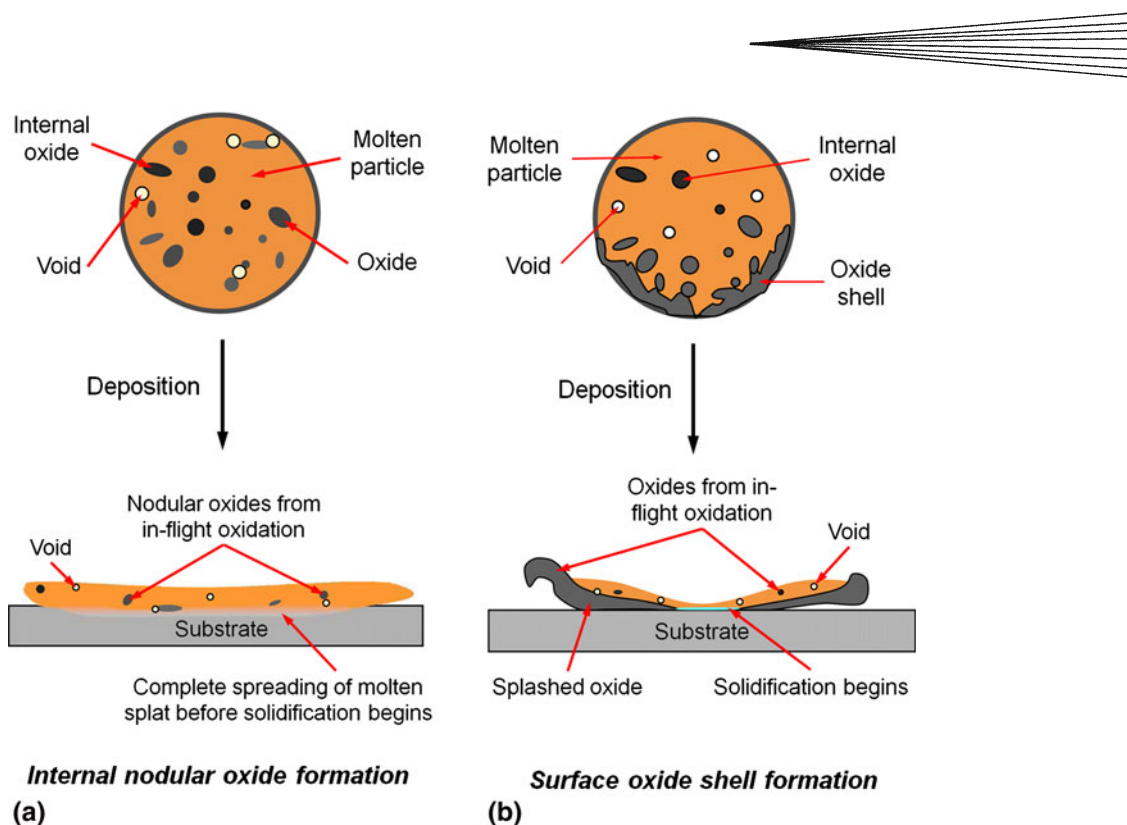


**Fig. 4** Schematics that illustrate in-flight oxidation. Molten particles and formation of the first splat with either (a) internal nodular oxides or (b) a surface oxide shell (Adapted from Ref 2)

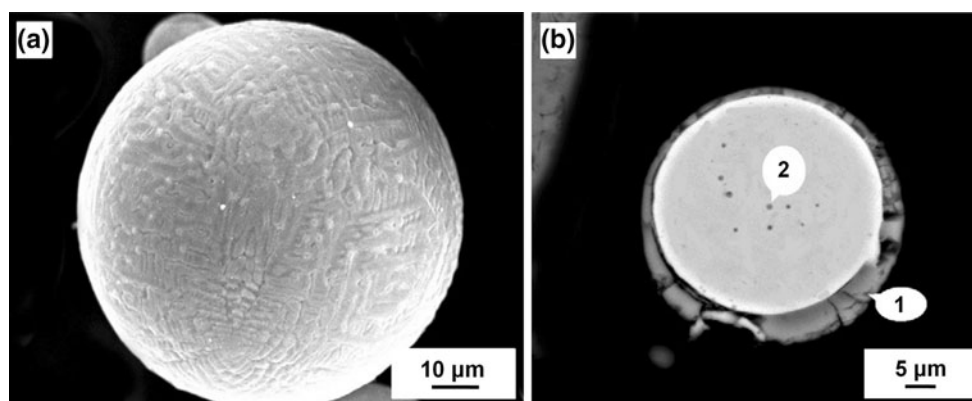


**Fig. 5** Micrographs of collected particles: (a) surface of particles collected at 55 mm and (b) cross section of particles collected at 120 mm. Points 1 and 2 represent the oxide shell and nodular oxide, respectively (Adapted from Ref 111)

standard experimental conditions (Ref 70). At distances further than this, the dominating mechanism is diffusion-based surface oxidation.

The oxides started to solidify and formed a thin oxide shell around the droplet as the particle temperature decreased, Fig. 4(b) and 5(b). Deshpande et al. (Ref 2) also proposed for the plasma spray process that oxides segregated toward the front end of the particle as the particle velocity increased due to the difference in relative velocity between the particle and plasma. The high radiation from the segregated oxides caused cooling at the front end of the particle. As a result, the

metal oxides in the droplets were pushed from the hot region toward the cooler front end by capillary flow to form an oxide cap, i.e., segregation of oxide at one end of the particle, Fig. 6. Syed et al. (Ref 70) also established that smaller particles promoted the entrainment of oxide toward the tail of the particle. Figures 5 and 6 highlight the formation of nodular oxides and surface oxide in collected sprayed particles. The presence of these oxides, in shell and nodular morphologies, has been verified by other researchers including Espie et al. (Ref 69), Sobolev and Guilemany (Ref 72), and Li and Li (Ref 73).

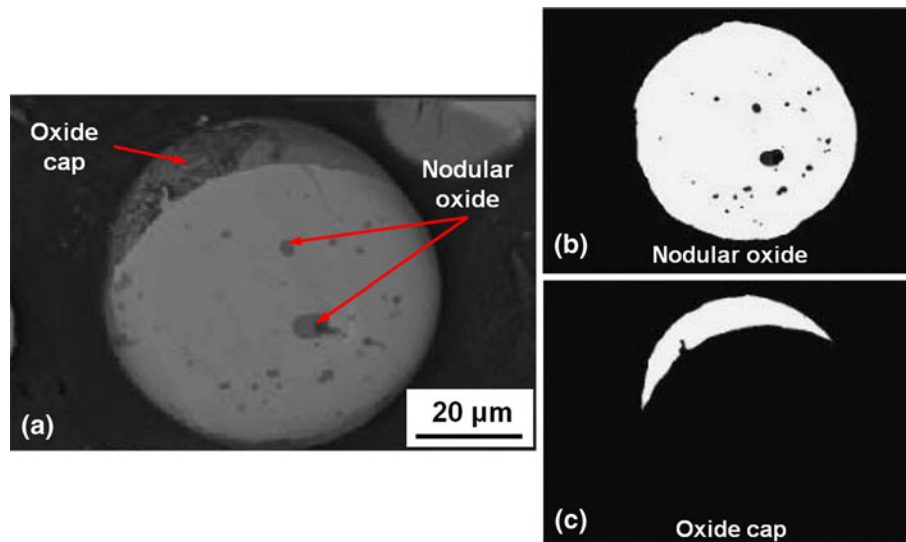


**Fig. 6** (a) Micrograph of the polished cross sections of a collected particle and image treatment analysis of (b) nodular oxides, and (c) oxide cap (Adapted from Ref 70)

In plasma spray, the in-flight oxidation of metallic particles is also influenced by the rate of particle evaporation, which occurs due to the high heat flux from the plasma gas (Ref 62, 74). The injected particles penetrate the plasma jet core and are rapidly oxidized and melted. The particle temperature continues to increase since the particles are within the hottest zone of the plasma. The particles would start to vaporize once they reach the boiling point of the material. The evaporated particles are either oxidized to the corresponding metal oxide or condensed in the form of metallic fume. In the case where the boiling point of the oxides is much lower than that of the pure material, such as tungsten, the oxides are evaporated at such a high rate that the coatings will be almost oxide-free. The rate of particle evaporation is determined by the partial pressure of oxygen in the boundary layer of the particles, which is restricted by the formation of an oxide mist that surrounds the particle. When the particles travel within the jet core, this oxide mist can be swept away by the gas flow around the particles, and the particles continue to evaporate. However, a less optimum particle trajectory will cause the partial pressure of oxygen to increase due to the buildup of counter-diffusing oxygen and metallic vapor at the particle surface (Ref 62). Consequently, the particle evaporation diminishes, and surface and nodular oxides continue to form as previously described. Therefore, the rate of oxidation is limited by the extent of particle evaporation.

Upon reaching the substrate, splats are formed on top of each other that are separated by alternating oxide layers as shown in Fig. 7. These oxide layers originated from the oxide shell formed during in-flight oxidation. The surface of the solidifying splat was exposed to a surrounding oxygen-rich atmosphere and, hence, can be further oxidized by the impinging jet until the splat was covered by the next arriving molten droplet, i.e., post-impact oxidation. According to Espie et al. (Ref 69), splat oxidation can be neglected since

the time lag for each splat to be covered by the next splat, and hence the time for splat exposure to the oxygen in the jet, is much shorter than the time lag between two successive passes. Each splat was covered by the next one within 10-20 μs, while a few seconds occur between two successive passes (Ref 31, 69). The splat layers are exposed to hot gases in the boundary layer flow that contains more than 90 vol.% of air between two successive passes (Ref 31, 61). On the other hand, Hackett and Settles (Ref 58, 75) believed that significant oxidation occurred after particle impact on the substrate.

The powder feed rate, torch traverse speed, deposition efficiency, and time between passes, which affect the time lag between the formation of two successive splats (Ref 2), play an important role in these opposing views. In addition, splat morphology influences the extent of post-impact oxidation. Splats with a higher surface area, such as fragmented splats, are oxidized to a greater extent than disk-shaped splats of the same volume under the same processing conditions.

In studying oxidation of a  $\text{Cr}_3\text{C}_2$ -NiCr coating, Matthews et al. (Ref 76) found that the splats were oxidized independently. That is, (i) carbide oxidation occurred by diffusion of oxygen through the oxide layer to the oxide-carbide interface, while (ii) oxidation of NiCr occurred by outward diffusion of chromium to the oxide-gas interface. Nickel oxide nucleated rapidly before being encapsulated from below by the slower growth of chromium oxide. The different oxidation mechanisms are attributed to the different structures of  $\text{Cr}_3\text{C}_2$  and NiCr. Unlike NiCr, the chromium atoms in  $\text{Cr}_3\text{C}_2$  are locked into the compound structure and are not free to diffuse out to the gas-oxide interface, hence resulting in the diffusion of oxygen into a carbide phase instead (Ref 76).

Zeng et al. (Ref 77) reiterated that spray distance greatly affected in-flight oxidation, while post-impact oxidation was influenced by particle size and substrate temperature. There is controversy concerning the

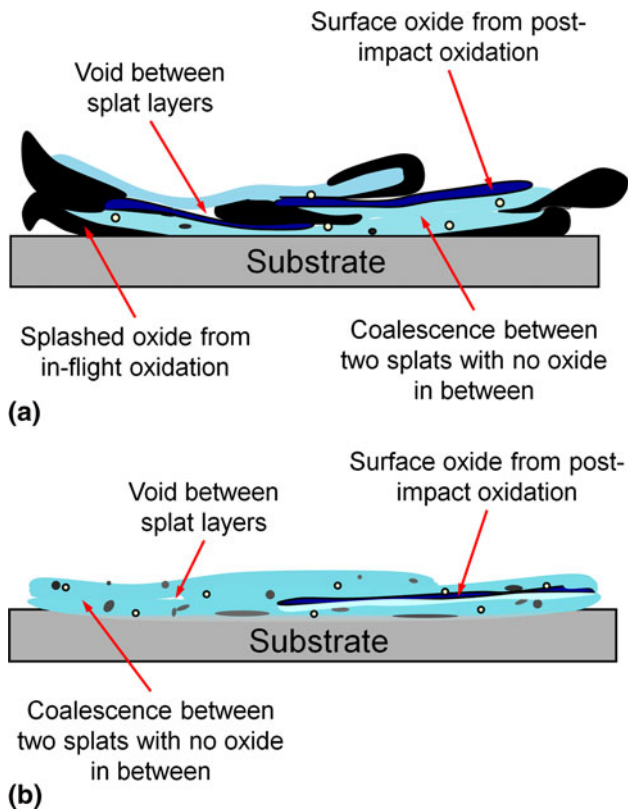
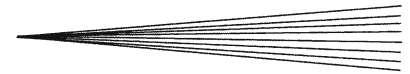


**Fig. 7** Schematics of consecutive splat formation on oxidized and non-oxidized regions of pre-deposited splat for (a) the atmospheric plasma spray (APS) process and (b) the high velocity oxy-fuel (HVOF) process (Adapted from Ref 2)

oxidation stage that dominates the thermal spray process. The oxidation process depends on the spray technique involved, spray parameters, and feedstock material. There is no single explanation that rules out the oxidation process. It is a complex process that involves many factors. Table 5 compares the various aspects of in-flight and post-impact oxidation in the thermal spray process.

## 4. Factors that Influence Oxidation

### 4.1 Types of Spray System

The factors affecting oxidation are governed by the type of oxidation process that is dominant. The oxidation process in control must be determined before the parameters can be adjusted to achieve the desired outcome. Oxidation is favored in both HVOF and plasma spray due to the presence of combustion product containing excessive oxygen in HVOF, the high temperatures involved in the plasma process (Ref 66), and mixing and entrainment with the ambient environment. The prevailing oxide varies for different spray techniques. Deshpande et al. (Ref 2) conducted a study on the oxidation of coatings sprayed under different techniques. It was found that APS and wire arc spray produced coatings with more porosity and oxides compared to

HVOF. This was due to the fact that in-flight oxidation was more extensive in APS and wire arc spray because of the longer residence time and greater degree of melting compared to HVOF. Fukushima and Kuroda (Ref 78) agreed with Deshpande et al. (Ref 2) that HVOF suppressed oxidation of metallic materials better than APS, whereas Knight and Smith (Ref 79) argued otherwise.

As pointed out earlier, oxides formed during the plasma spray process segregated toward the front end of the particle due to relative velocity effects. On the contrary, the lower temperature of HVOF led to higher viscosity and a lower relative velocity difference between the flame and the particle, thus resulting in internal oxides and a thin oxide shell, but no oxide segregation. Post-impact oxidation was also more pronounced for an APS coating, while only thin oxide bands were observed for a HVOF coating due to the reduced exposure time of the previous splat.

The level of oxidation observed for HVOF coatings varies with respect to the different HVOF systems. The JP-5000 system (Praxair Surface Technologies, IN, USA) reduced oxygen content using over-stoichiometric conditions, while an under-stoichiometric condition was needed to attain low oxygen contents when using the Diamond Jet (DJ) Hybrid systems (Sulzer Metco, Wohlen, Switzerland) (Ref 59). This variation was attributed to the different fuels used in each system and hence different combustion products and temperature. The two systems showed contrasting effects on oxidation due to their distinctive powder injection position. Feedstock powder was injected directly into the combustion chamber, before the de Laval nozzle, in a DJ Hybrid system. On the other hand, in the JP-5000 system, the feedstock was injected after the combustion chamber, leading to lower temperatures in the system. The position of powder injection was important since it determined the type of oxidation that dominated. In-flight oxidation dominated for traversing particles, while post-impact oxidation prevailed for external powder injection techniques (Ref 75). The lower temperature system resulted in lower melting that reduced the degree of splashing during the splat quenching process. In this manner, the surface area exposed to the atmosphere decreased, and hence there was less oxidation. Nonetheless, the oxidation level was still influenced by the effects of other parameters such as the oxygen/fuel (O/F) ratio, chamber pressure, gas flow rate, particle size, and spray distance.

Another example of differing spray system and injection position effects on the dominating oxidation process is the coatings produced by gas-stabilized plasma (GSP) and water-stabilized plasma (WSP). Although the coatings sprayed by both techniques exhibited similar oxygen content, the oxide morphologies of the coatings vary significantly. The GSP coatings contain mainly nodular oxides with a very thin oxide shell (less than 100 nm), while the WSP coatings contain a thick oxide shell with no nodular oxide (Ref 69). The oxide shell in WSP low carbon steel coatings was two to four times thicker than that of GSP coatings. Such difference in oxide morphologies was attributed to variation of injection position. The particles have to be injected further downstream (65 mm from exit nozzle) for WSP compared to GSP (3 mm from

**Table 5 Comparison of in-flight and post-impact oxidation in thermal spray process**

In-flight	Region(s)	Post-impact
<ul style="list-style-type: none"> <li>I: Jet core</li> <li>II: Beyond jet core, where local atmosphere is entrained into the flame centreline</li> <li>I: Gas-solid (unmolten particles)</li> <li>II: Gas-liquid (molten particles)</li> <li>• Amount of entrained air (jet velocity)</li> <li>• Particle temperature</li> <li>• Particle velocity</li> <li>• Nature and turbulence of flame</li> </ul>	III: Splats on substrate between two successive layers  III: gas-solid (splats)  Oxidation phase(s)  Influencing factors  Oxide forms  Mechanism	<ul style="list-style-type: none"> <li>• Time lag between two successive splats:               <ul style="list-style-type: none"> <li>◦ Powder feed rate</li> <li>◦ Torch traverse speed</li> <li>◦ Deposition efficiency</li> <li>◦ Time between passes</li> </ul> </li> <li>• Splat morphology</li> <li>• Surface oxides between splat layers</li> </ul> Diffusion-based to form surface oxides (either inward or outward, depending on the material)

exit nozzle) to reduce vaporization of particles (Ref 69). Consequently, the Reynolds number for particles in GSP was more than four times that for particles in WSP, and hence there was more convective movement within the particles that caused the formation of nodular oxide. The oxide shell in WSP coatings was much thicker since the particles travel a greater distance and at a lower velocity compared to the GSP process, which allows more time for the growth of the oxide shell.

#### 4.2 Oxygen-to-Fuel Ratio and Current Intensity

The O/F ratio was considered the most influential parameter that affected oxygen content for a HVOF-sprayed coating (Ref 59). As mentioned earlier, different spray systems have varying O/F ratio effects on oxidation, and the under-stoichiometric condition does not necessarily favor oxidation. There are opposing opinions concerning the influence of the O/F ratio on oxidation. On the one hand, it was proposed that increasing the O/F ratio decreased oxidation because combustion temperature decreased (Ref 75). Voggenreiter et al. (Ref 80) established that the particles must be sufficiently cold so that fragmentation does not occur upon impact since molten particles would tend to fragment upon impact and create an increased area that would be liable to oxidize. On the other hand, decreasing the O/F ratio decreased oxidation since excess oxygen was minimized at a low O/F ratio (Ref 81). The reduction of excess oxygen directly diminished in-flight oxidation.

Syed et al. (Ref 64, 65) investigated the effect of current intensity and the hydrogen ratio of plasma spray on in-flight oxidation. Figure 8 shows the effects of current intensity and hydrogen flow rate on the oxygen content as well as formation of nodular oxides and oxide cap. It was found that higher current intensity favored in-flight oxidation and the formation of nodular oxides. An increase of current intensity led to a rise of temperature as well as the particle velocity, Fig. 8(a). Shorter dwell time and high velocity led to a decrease of surface oxide formation, while the particle Reynolds number and convective reactivity of particles escalated so that more nodular oxides were formed. Since surface oxides were dominant in this case, the total oxide content decreased even though the amount of nodular oxides increased, Fig. 8(c). The rise in hydrogen ratio also enhanced the formation of nodular oxides, while formation of an oxide shell increased sharply and then deteriorated gradually, Fig. 8(d). A higher hydrogen flow rate encouraged the surface oxides of molten particles to penetrate the powder in-flight and led to many nodular oxides inside the powder after solidification (Ref 82).

#### 4.3 Gas Flow Rate

Generally, an increase of gas flow rate is expected to cause an increase in the flow momentum of either a plasma plume or a HVOF flame and hence an increase in particle velocity and a decline in oxidation. However, the interaction between the different gases involved in both

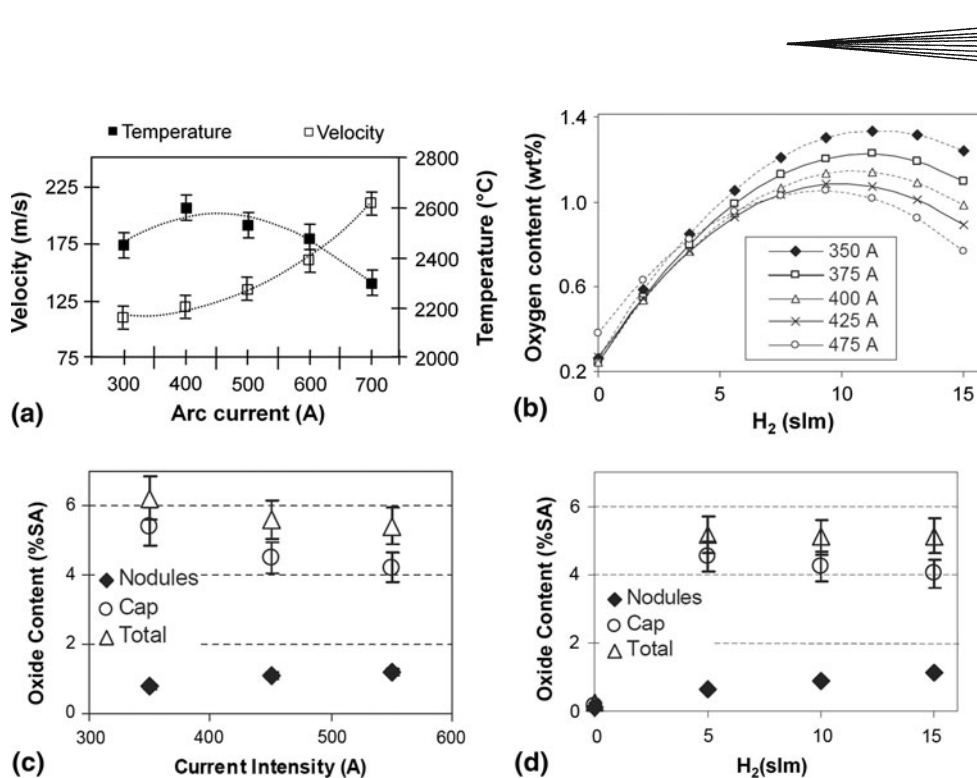


**Fig. 8** (a) Effects of current intensity on in-flight particle temperature and velocity (Ref 117), (b) effects of current intensity and hydrogen flow rate on the oxygen content (Ref 65), (c) percentage area of oxide nodules and oxide cap as a function of current intensity (Ref 65), and (d) percentage area of oxide nodules and oxide cap as a function of hydrogen flow rate (Ref 65)

plasma spray and HVOF systems, i.e., primary and secondary plasma-forming gases, combustion gases, and carrier gas, is complex. The effects of flow rates of these gases on the particle characteristics and degree of oxidation are interdependent.

The total gas flow rate has little effect on the gas velocity and temperature within the nozzle since they are limited by the nozzle and are considered to be at a choking state (Ref 83). However, a high total gas flow rate will increase the mass flow rate of the free jet at the nozzle exit. The increased mass flow rate causes an increase of total thermal and momentum inertia, where the flame gas can be kept at high temperature and velocity for a longer distance. The effects of total gas flow rate are valid for both plasma spray and HVOF systems where the increase of total gas flow rate of (i) the primary and secondary gases in plasma spray, and (ii) the oxygen and fuel gases in HVOF, increases the ratio of heat-generating gas to non-heat-generating gases such as the carrier gas. Since the particle temperature and velocity both influence oxidation through the effects of degree of melting and in-flight time, respectively, the extent of oxidation will depend on the type of dominating oxides as discussed in section 4.2.

In a plasma spray system, an increase in the primary gas flow rate imparts a greater momentum to the in-flight particle, hence increasing the particle velocity and decreasing the in-flight time. Also, the increase of plasma jet velocity constricts the penetration of particles fed radially into the jet core, therefore lowering the particle temperature. Increasing the primary gas flow rate, while maintaining the secondary gas flow rate, also decreases the plasma energy density and particle temperature since the

fraction of secondary gas that generates greater enthalpy is lowered (Ref 84). The shorter in-flight time and lower particle temperature induced by the increase of primary gas flow rate results in reduced oxidation.

On the other hand, the secondary gas flow rate did not alter greatly the plasma temperature and velocity. However, the thermal conductivity and plasma-to-particle heat transfer increased distinctly (Ref 64). Planche et al. (Ref 85) also suggested the same mechanism, but claimed that the increase in hydrogen flow rate led to higher temperature and better melting. Greater heat transfer magnified particle temperature until a point where an asymptotic limit was reached where further changes in average particle temperature became negligible (Ref 64). Once this temperature was reached, hydrogen served as a reducing species and reacted with the highly oxidizing species in the plasma jet, hence decreasing oxidation. While each powder exhibited a different melting state, Kim et al. (Ref 82) also agreed with Planche et al. (Ref 85) that an increase in hydrogen flow rate boosted the fraction of molten feedstock in the plasma, i.e., the lamellar structure of splats increased with hydrogen flow rate. Hydrogen flow rate had almost no influence on particle velocity independent of the particle size, while the rise in particle temperature became more significant as the particle diameter increased.

An increase in the carrier gas flow rate increases the particle velocity, but at the same time the gas temperature is lowered since the carrier gas absorbs the thermal energy generated by the plasma-forming or combustion gases (Ref 83, 86). Consequently, the heat transfer to the particle and degree of melting are lowered, the in-flight time is shortened, and the extent of oxidation is diminished.

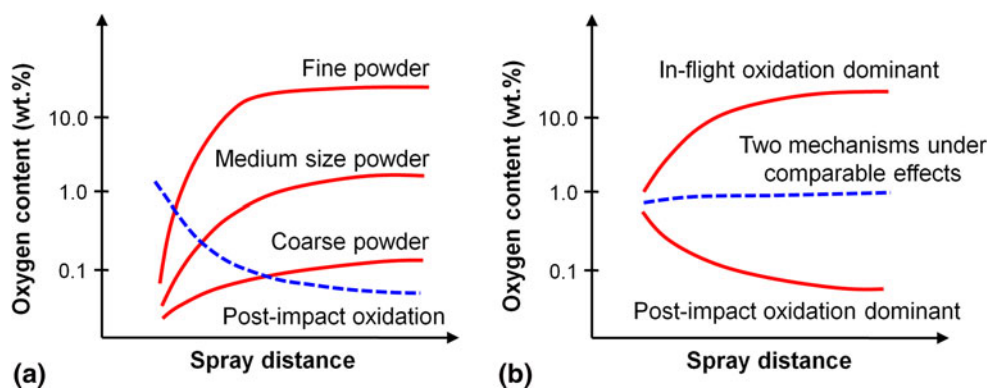


**Fig. 9** Diagram illustrating the dependency of oxygen content in a coating on the spray distance in terms of different (a) particle sizes and (b) dominating oxidation process (Adapted from Ref 73)

#### 4.4 Particle Size

The studies by Gourlaouen et al. (Ref 87, 88) and Fukushima and Kuroda (Ref 78) showed different degrees of oxidation, although both groups used the same spray process and material. It has been established that particle size plays a significant role in this discrepancy. Contradicting findings on the effects of particle size on oxidation of thermal spray coatings have also been noted. Effects of particle size on oxidation depend on the type of oxidation that dominated. Generally, oxidation was enhanced when the particle size decreased if in-flight oxidation was in control (Ref 2, 64, 72, 89, 90). The reasoning was that the smaller particle size provided a higher surface area and hence more exposure to oxygen in-flight. In addition, Sobolev and Guilemany (Ref 72) recommended the use of feedstock with a narrow size distribution and large mean size of particles to reduce oxidation.

Li and Li (Ref 73) found that oxygen content did not change much for particle sizes below 45  $\mu\text{m}$ . On the contrary, oxygen content increased exponentially with decreasing particle size by a power of approximately 3.4 for particles larger than 45  $\mu\text{m}$ . It was suggested that there was a transient particle size range where the dominant mechanism changes, and this was reflected in the oxidation effects on the particles. The size range depended on the spray conditions. For larger particle sizes, post-impact oxidation was responsible for the oxygen content in coatings. However, it was claimed that the contribution of post-impact oxidation to total oxygen content in the coating was significant only when the total oxygen content in the coating was low. In other words, in-flight oxidation was almost always the major type of oxidation. This claim was supported later by Espie et al. (Ref 69). Figure 9(a) (Ref 73) shows the effect of particle size on the oxygen content in coatings as a function of spray distance.

#### 4.5 Spray Distance

Spray distance or standoff distance was another important parameter that determined the extent of oxidation in a coating. As mentioned in section 3.2, the mechanism of oxidation was proposed to change from convective to

diffusion when the spray distance increased, thus resulting in the formation of nodular oxides and an oxide shell, respectively. Figure 10 shows the type of oxides observed in collected particles sprayed at different spray distances.

Espie et al. (Ref 91) found that the oxygen content of plasma sprayed low carbon steel particles increased with spray distance. Zeng et al. (Ref 77) presented comparable results on plasma sprayed iron and NiCr-based alloys. Although Fukushima and Kuroda (Ref 78) reported similar results on plasma sprayed Ni-20Cr, a HVOF-sprayed stainless steel coating showed the opposite effect. Once again, the dominating oxidation process, i.e., in-flight or post-impact, played an important role. The changes in oxygen content as a function of spray distance for in-flight oxidation and post-impact oxidation are shown in Fig. 9(b) (Ref 73). In cases where in-flight oxidation was in control, a short spray distance reduced oxidation because particles spent less time in the flame and were less exposed to in-flight oxidation. On the other hand, in situations where post-impact oxidation matters more, a longer spray distance minimized oxidation since the temperature on the substrate surface was reduced with the heat source further away.

#### 4.6 Substrate Temperature and Heat Treatment

Substrate temperature did not affect in-flight oxidation, but it influenced post-impact oxidation (Ref 77). Hackett and Settles (Ref 75) demonstrated that oxidation was enhanced when the substrate temperature was high. A high substrate temperature impeded the solidification process and hence exposed the molten splat to the surrounding atmosphere for a longer time. On the contrary, Espie et al. (Ref 69) contended that substrate temperature control did not affect oxygen content of the coating significantly, but it led to better adhesion between the coating and substrate. The improved adhesion was proposed to be caused by the formation of an appropriate oxide layer on the substrate.

Heat treatment of a coating often led to intersplat sintering and the disappearance of splat boundaries (Ref 76). Post-spray heat treatments also reduced the hardness of the coating, while metallurgically enhancing

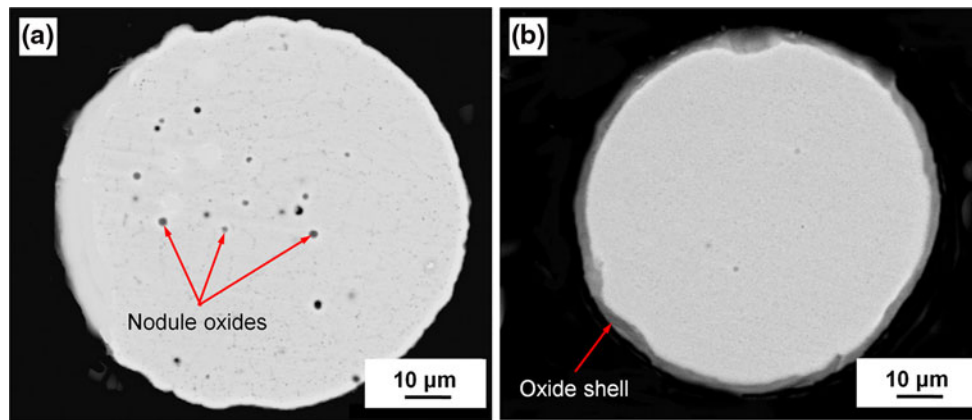
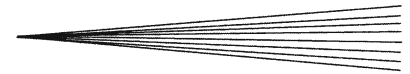


**Fig. 10** Micrographs of particle cross sections showing the effects of spray distance on the dominating type of oxide: (a) nodular oxides for particles collected at 55 mm and (b) oxide shell for particles collected at 75 mm (Adapted from Ref 111)

the bond strength. The fine grain microstructure and enhanced bond strength helped prevent corrosive liquids from penetrating the coating between particles. In other words, oxygen may also be prevented from entering the voids between particles and, hence, mitigate against oxidation during any aging process. In terms of oxides, heat treatment was claimed to break off the continuous surface oxide layer and form oxide spheres (Ref 59). It was suggested that the oxide spheres filled the spaces between particles and improved the bond strength.

In short, the oxidation process can be controlled by manipulating the process parameters provided that the mechanism and the dominating oxidation process are understood. Generally, the extent of oxidation is regulated by two main factors: (i) the in-flight time or particle velocity and (ii) the degree of melting or particle temperature. These two factors can be used to control oxidation concurrently or separately and are dictated by the variables discussed in section 4. Firstly, oxidation can be limited by shortening the particle in-flight time or increasing the particle velocity so that the time available for reaction between the particles and oxygen is limited. This can be achieved using (i) a high velocity process such as HVOF, (ii) a high current intensity, (iii) a high total, primary, and/or carrier gas flow rate, and/or (iv) a short spray distance.

Alternatively, a low level of oxidation can be achieved by lowering the degree of particle melting or the particle temperature, where the reactivity of the particle with oxygen is limited. This condition can be established using (i) a lower temperature process, (ii) feedstock injection after the combustion chamber, (iii) a low current intensity, (iv) a high primary and/or carrier gas flow rate, (v) a low total and/or secondary gas flow rate, (vi) a large mean particle size with narrow particle distribution, and/or (vii) a low substrate temperature. Particle temperature can also be lowered for the HVOF process using a high O/F ratio, but care is required when exercising this approach since it also creates an oxidizing environment that will enhance oxidation. The extent that these process parameters influence the oxidation differs and will further depend on

the type of dominating oxidation process, i.e., in-flight or post-impact.

## 5. Protection Against Oxidation During Processing

Metals and alloys deposited by thermal spray processes can have some level of protection against oxidation (Ref 69). Such protection strategies include the following:

- Shrouding with a combustible gas such as acetylene.
- Effective use of a non-combustible protective gas.
- Maintaining the substrate at the lowest possible temperature that is compatible with good adhesion/cohesion.
- Rapid cooling.
- Use of a vacuum or controlled atmosphere chamber to evacuate air.

Alloy powders have been sprayed with the high velocity air-fuel (HVOF) process and cold spray to prevent oxidation (Ref 92, 93). Oxidation was greatly reduced, but the coating density tended to be inadequate and post-spray sealing was usually required. Spraying under vacuum conditions was effective, but at the expense of an increased processing cost. Also, generating a vacuum medium was time consuming and the size of the parts to be created was restricted by the chamber size. As a result, many researchers have employed gas shrouding, and this has proved to be effective and relatively inexpensive.

### 5.1 Gas Shroud Versus Gas Shield

Protection measures against oxidation have been implemented as early as in the 1960s. Patents have been filed on varying designs of shields and shrouds for thermal spray purposes (Ref 94-97). Schematics of these gas shroud designs are shown in Fig. 11. Both gas shield and shroud are components that are flushed with inert gas during operation

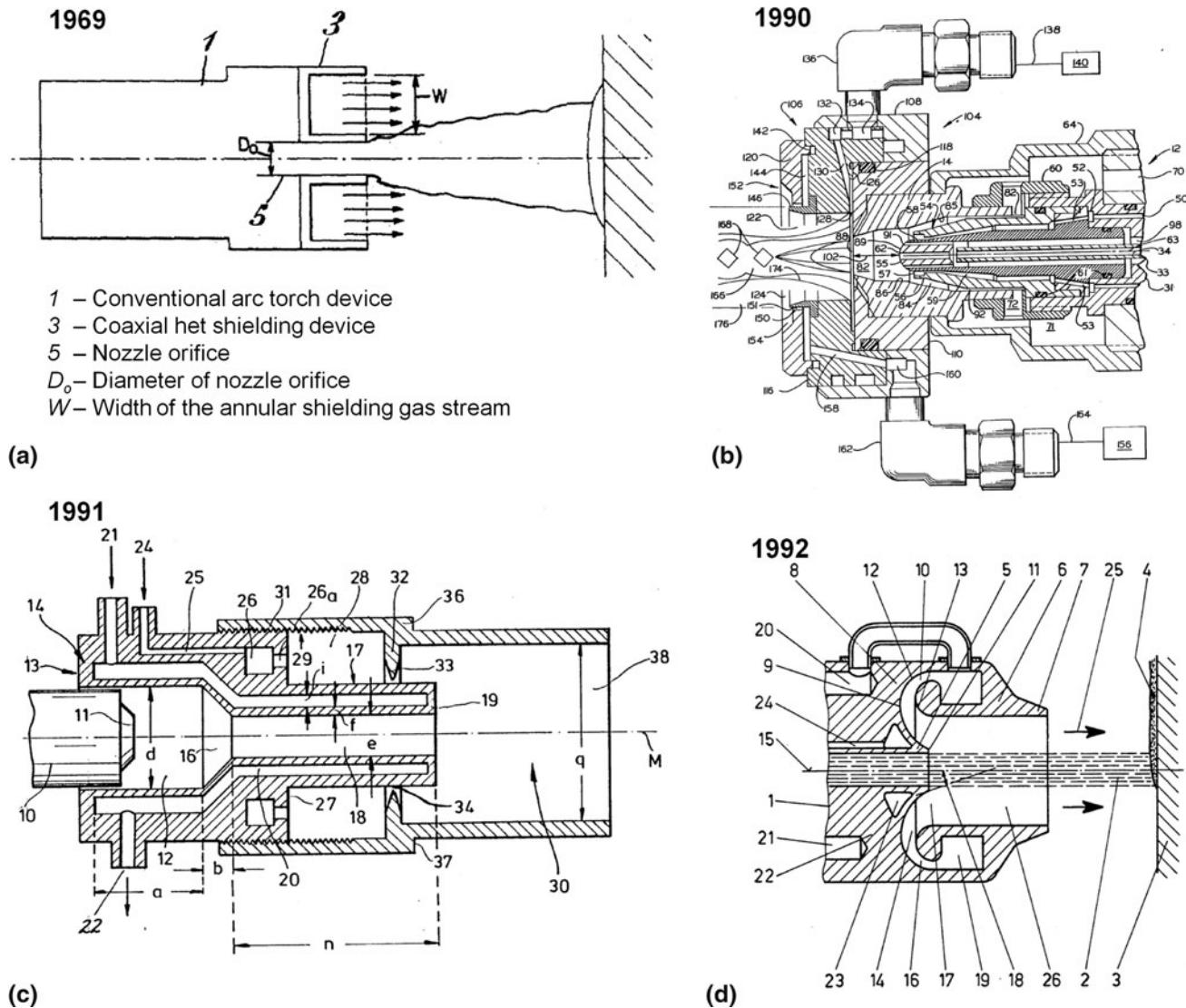


**Fig. 11** Schematic of several gas shroud patents designed for thermal spray by (a) Jackson, Union Carbide Corporation (Ref 94), (b) Rotolico and Weodarczy, The Perkin-Elmer Corporation (Ref 95), (c) Simm, Steine, and Streb, Castolin S.A. (Ref 96), and (d) Reiter, Nova-Werke AG (Ref 97)

for oxidation protection, which differ in their attachment position, i.e., a shield is attached to the substrate surface, while a shroud is attached to the thermal spray source.

Jackson (Ref 94) used argon and helium gases as shielding gas to reduce the oxygen concentration in coatings. This type of protection has been used for various thermal spray techniques such as plasma spray, wire arc, and also HVOF. Figure 12 shows the comparison of the oxide contents in coatings sprayed with and without a gas shroud. The type of protection used, however, depends greatly on the oxidation process involved, i.e., whether oxidation was dominated by in-flight or post-impact mechanisms. In cases where in-flight oxidation dominated, a gas shroud was a good option, while at times where post-impact oxidation was in control, a shield must be used.

Shield and shroud methods have been presented by Fukushima and Kuroda (Ref 78), Fig. 13.

Mostaghimi and co-workers developed a cylindrical shroud that successfully minimized in-flight oxidation. However, the shrouded nozzle causes recirculation of flow within the nozzle and decreases the particle velocity (Ref 98). In addition, the recirculation of cold air at the exit of a conventional conical gas shroud nozzle reduces the plasma enthalpy and the particle temperature (Ref 99). The Mostaghimi group further developed a curvilinear insert to the gas shroud nozzle that conformed to the streamlines of the primary gas flow and eliminated the air recirculation (Ref 99, 100). This modification impeded mixing with the surrounding atmosphere and improved the heat and momentum transfer to the particles.

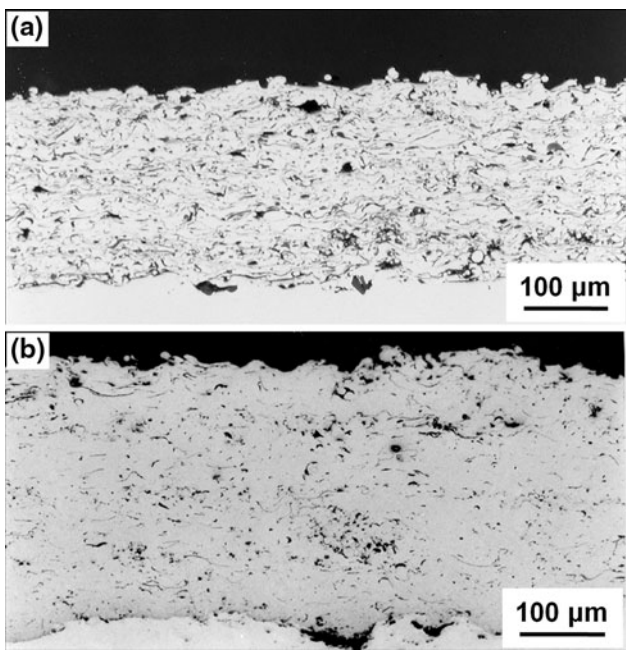


**Fig. 12** Cross section of plasma sprayed CoNiCrAlY coatings sprayed (a) without and (b) with nitrogen shrouding (Adapted from Ref 118)

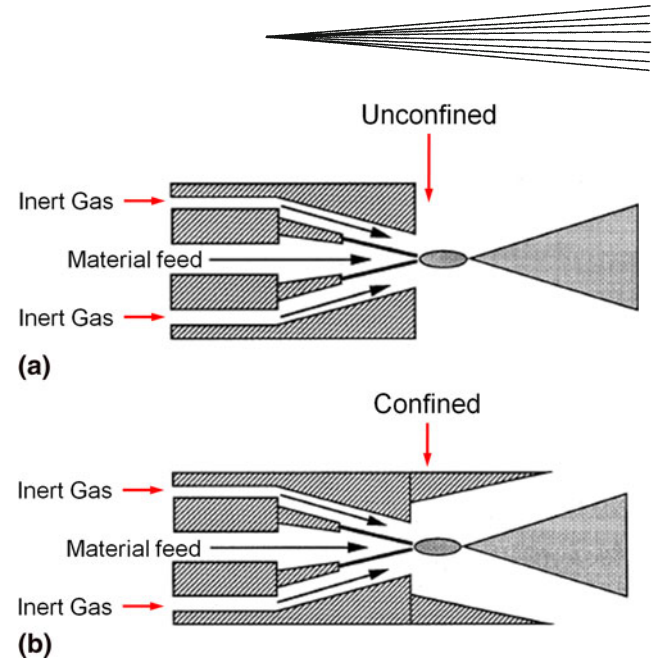


**Fig. 14** Schematics of nozzle and shroud configuration for (a) straight bore nozzle with shroud inert gas protection and (b) straight bore nozzle with secondary gas injection (Adapted from Ref 101)

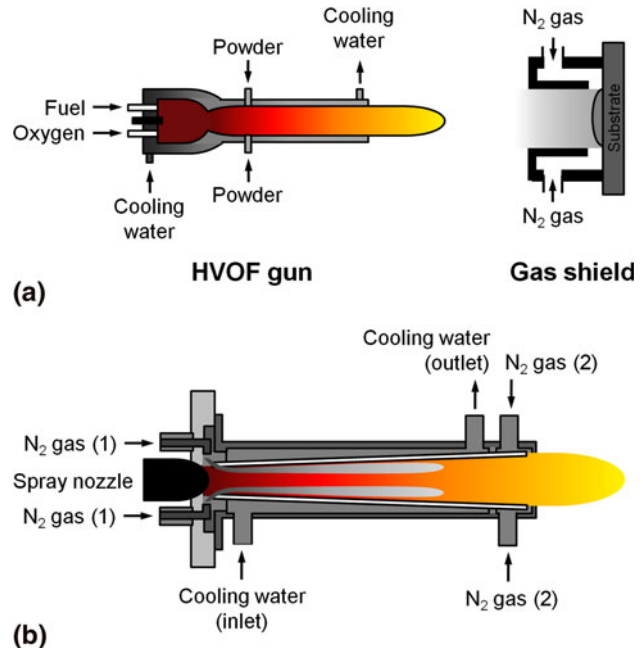


**Fig. 13** Schematics of two types of gas shielding attachments used to control oxidation: (a) nitrogen gas shielding attachment used on a substrate and (b) gas shroud used to control the oxidation of HVOF-sprayed particles during in-flight (Adapted from Ref 78)

In the process of understanding coating oxidation control, Hackett and Settles (Ref 58) used Schlieren images to visualize the operational mechanics of gas shrouding. It was shown that the shroud gas flows coaxially

to the HVOF jet from the spray torch and was rapidly entrained. The extent of the entrainment was indicated by limiting the streamline between the shroud gas and the ambient atmosphere. Further downstream of this point, the ambient atmosphere became entrained into the jet. The inert shroud gas became distributed throughout the mixing layer by vigorous turbulent mixing. This mechanism served to dilute the amount of oxygen present in the jet centreline. The effects of gas properties and flow rate will be discussed further. Hackett and Settles (Ref 58) established that shrouding controlled the formation of coating oxides and also reduced the oxidation levels in iron coatings by as much as 50 wt.%. Wang et al. (Ref 101), who implemented two types of shrouding on the wire arc spray process, also verified the same outcome. An unconfined shroud demonstrated higher oxide levels due to air entrainment. Spraying in a confined gas shroud also resulted in more uniform particle size distributions, more focused spray patterns, higher particle velocities, and improved coating properties (Ref 101). Figure 14 shows the gas shroud configuration used by Wang et al. (Ref 101) where Fig. 14(a) shows an unconfined shroud, while Fig. 14(b) is confined.

Hackett and Settles (Ref 58) demonstrated that coatings sprayed using a ducted controlled atmosphere spray (CAS) has lower oxygen content than the coatings sprayed using an unconfined shroud for the same gas mass flow rate. In other words, the working area of a gas shroud around the torch must be enclosed for better efficiency. Wang et al. (Ref 101), who implemented two types of shrouding on the wire arc spray process, also verified the same outcome. An unconfined shroud demonstrated higher oxide levels due to air entrainment. Spraying in a confined gas shroud also resulted in more uniform particle size distributions, more focused spray patterns, higher particle velocities, and improved coating properties (Ref 101). Figure 14 shows the gas shroud configuration used by Wang et al. (Ref 101) where Fig. 14(a) shows an unconfined shroud, while Fig. 14(b) is confined.

**5.2 Selection of Inert Gas**

Inert gases, such as argon, nitrogen, and helium, are normally used as shroud gases. Hackett and Settles

(Ref 58) compared the effect of different gases for shrouding on oxidation and concluded that the choice of shroud gas had little influence on the oxygen content in the coating. An argon-shrouded coating exhibited a similar oxygen content to a nitrogen-shrouded coating at the same shroud gas mass flow rate. A helium shroud produced the lowest oxygen content coatings at a low shroud gas mass flow rate, taking note that the volume flow rate was equivalent to the highest nitrogen flow rate due to the low density of helium ( $0.17 \text{ kg/m}^3$  for helium compared to  $1.17 \text{ kg/m}^3$  for nitrogen and  $1.66 \text{ kg/m}^3$  for argon). Thus, coatings produced under nitrogen and helium shrouds exhibited similar oxygen levels at the same volume mass flow rates.

An interesting study by Volenik et al. (Ref 63) used acetylene ( $\text{C}_2\text{H}_2$  with a density of  $1.09 \text{ kg/m}^3$ ) as a shroud gas instead of the conventional inert gases. It was found that nitrogen-hydrogen shrouding was less effective in decreasing oxide contents and the oxide layers were thicker with pronounced dendritic growth. A combustible gas, acetylene, on the other hand demonstrated a twofold effectiveness in reducing the oxide levels. Acetylene worked because it displaced air and reduced the amount of oxygen available in the plume by consuming it in a combustion process. The use of carbon dioxide ( $\text{CO}_2$  with a density of  $1.84 \text{ kg/m}^3$ ) as a gas shroud instead of the conventional inert gases has also been found effective by Wang et al. (Ref 102). The oxide content of the stainless steel coatings decreased by 15 wt.% when produced under a carbon dioxide shroud.

Kang and Hong (Ref 103) found that a shroud gas flow rate 3.75 times that of the torch working gas was necessary to achieve a “nearly oxygen-free plasma” region with an air content of approximately 10 mol.% at 100 mm downstream of the nozzle exit. Gawne et al. (Ref 104), on the other hand, showed that the air content can be reduced from 82 to 46 vol.% with a 100 m/s velocity shroud gas at the turbulent jet center, 105 mm from the torch nozzle exit. Hackett and Settles (Ref 58) found that an increase in gas shroud mass flow rate completely enveloped the HVOF jet and very little atmospheric oxygen was entrained. Despite this, some minimum amount of oxygen was always present in coatings due to either (i) free oxygen combustion in Region I (refer Fig. 1) or (ii) oxides that were present in the feedstock powder. It was also found that an increase in the inert shroud gas mass flow rate resulted in a linear decrease in oxygen content.

It has been established that the gas shroud and/or shield can affect the temperature, velocity, and air concentration fields in turbulent plasma jets. While gas shrouding was very effective in minimizing oxidation, Dolatabadi et al. (Ref 98) claimed that the coatings were more porous due to a reduction in particle impact velocity. On the contrary, Wang et al. (Ref 101) disagreed and found that shrouding reduced the porosity level in coatings. Instead of reducing particle impact velocity, Wang et al. (Ref 101) argued that shrouding accelerated the droplets and air entrainment caused less cooling. Hence, the coating was built up at higher velocity and

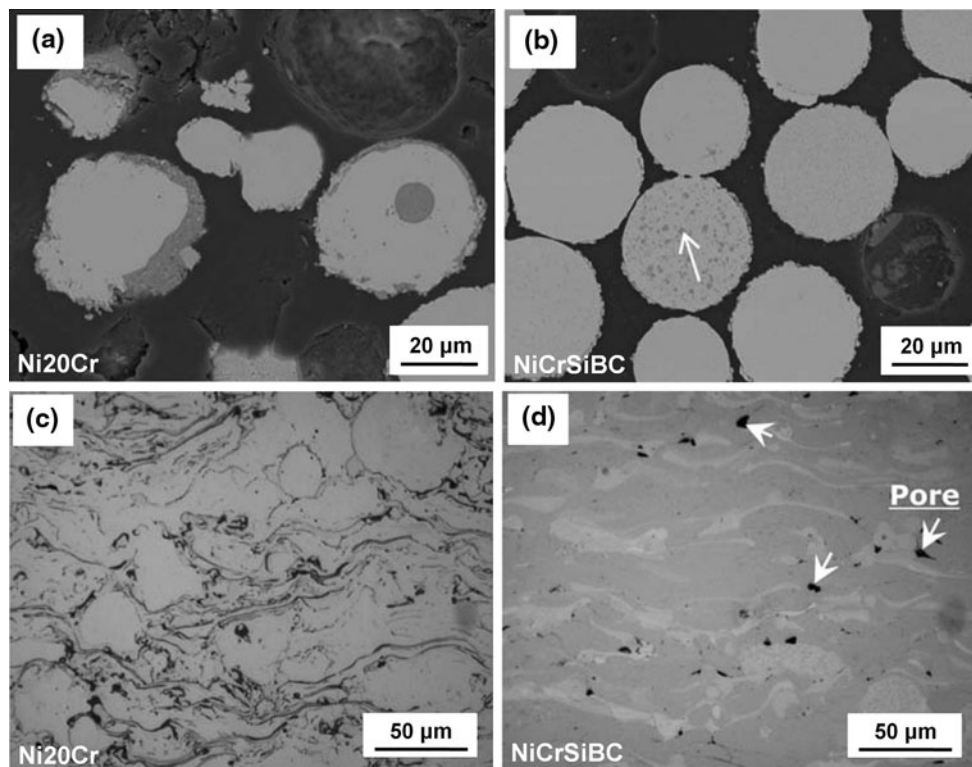


**Fig. 15** Cross-sectional images of captured particles and coatings depicting the effects of SEs: (a) and (c) without SEs, (b) and (d) with silicon and boron as SEs (Adapted from Ref 77)

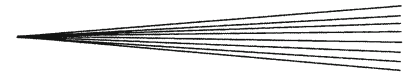


**Table 6** Examples of thermal spray powders that implemented the concept of “SE”

	Composition, wt. %				Reference
	BM	SE	BM	SE	
(i) Coated particles	Molybdenum	Nickel	38.0-62.5%	37.5-62.0%	119
	Nickel, copper, or iron	Aluminum and molybdenum	66.0-97.5%	2-18% Al, 0.5-16.0% Mo	120
	Cast iron	Molybdenum and boron	Balance	10-50% Mo, 0.1-3% B	121
	Nickel or cobalt, with boron	Aluminum	66-99% (1-6% B)	1-34%	122
	Nickel, iron, or cobalt, with chromium or aluminum	Aluminum and cobalt	Balance(1-55% Cr or Al)	1-15%	123
	Nickel, iron, cobalt, and/or chromium	Aluminum and yttrium oxide	Balance	1-15% Al, 0.5-10% Y <sub>2</sub> O <sub>3</sub>	124
	Ni, Fe, Co, Cu, and/or Cr with Al, Y, Hf, and/or Lanthanides	Al, Fe, and Cu	70-96% (15% Al, Y, Hf, and/or Lanthanides)	3-20% Al, 0.5-10% Fe, Cu	125
	MCrAlY (M = Fe, Ni, Co, Fe-base, Ni-base, Co-base)	Aluminum	Balance	1-50%	126
	Ni, Co, Fe, Cu, Ni-base, Co-base, Fe-base, Cu-base, and/or aluminum bronze	Oxidizable metal (Fe, Co, Ni, Cu, Al, Be, Si, Sb, Zr, Mo, and/or W)	Balance	2-20%	108
	Nickel or cobalt	Boron and/or silicon	Balance	5-15%	127
(ii) Powder mix or agglomerates	MCrAlY-X (M = Ni, Co and Fe)	X = Hf, Rh, La, Ta	20-35% M, 5-15% Al, 1-6% Y	2-10% X	128

**Table 7** Hardness values of various metals and their oxides (Ref 129)

Metal	Hardness, kg/mm <sup>2</sup>	Metal oxide	Hardness, kg/mm <sup>2</sup>
Aluminum	15	Al <sub>2</sub> O <sub>3</sub>	1800
Chromium (plated)	850	CrO <sub>3</sub>	1600
Copper	40	Cu <sub>2</sub> O, CuO	130
Iron	105	FeO, Fe <sub>2</sub> O <sub>3</sub> , Fe <sub>3</sub> O <sub>4</sub>	400
Lead	5	PbO, PbO <sub>2</sub>	250
Magnesium	27	MgO	400
Molybdenum	220	MoO <sub>3</sub>	50
Nickel	86	NiO, Ni <sub>2</sub> O <sub>3</sub>	430
Tin	5	SnO <sub>2</sub>	1650
		SnO	350
Zinc	35	ZnO	200

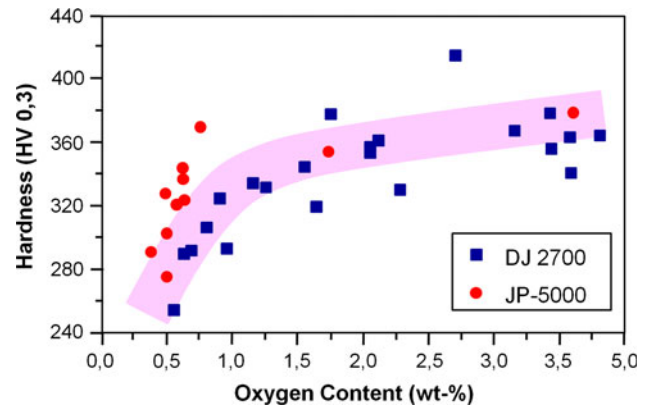


**Fig. 16** Variation of Vickers hardness values with oxygen content in high velocity oxy-fuel-sprayed stainless steel 316L coatings (Adapted from Ref 59)

temperature that led to reduced porosity. It was established that shrouding reduced the amount of oxides and there was more uniform contact between the metallic splats. Planche et al. (Ref 85) also agreed that coatings from shrouded spraying were less porous than conventionally sprayed coatings due to the increase in temperature and velocity in the shroud.

The above contradicting views are attributed to the difference in materials, nature of gas shroud used, and the flow rate. In all cases, each shroud must be designed specifically according to the spray gun used so that oxidation can be reduced and, at the same time, any adverse effects of using such a shroud can be minimized. The optimum geometry must be used to achieve this. Modeling and theoretical computation have been performed for different shroud designs (Ref 103-106) to verify the effectiveness of gas shrouding as well as to design the ideal shroud geometry.

### 5.3 Sacrificial Elements

Besides gas shrouding, some light alloying elements, such as silicon and boron, can be added as “sacrificial elements” (SEs) in the feedstock. The SEs must (i) readily

react with oxygen to form oxides and (ii) exhibit greater affinity to oxygen than the core elements. Figure 15 shows the effects of SEs on the reduction of oxidation for collected sprayed particles and coatings. The reduction of on-substrate oxidation becomes more obvious with the increase of SE content. Zeng et al. (Ref 77, 107) found that the SE content was reduced in captured in-flight particles and coatings compared to the feedstock, but revealed no difference between the captured particles and coatings. To look at this another way, the addition of such SEs was more effective against in-flight oxidation than for post-impact oxidation. Boron was found to be the most effective SE against the oxidation of iron. However, extra precautions must be taken when using such SEs because the oxidation of such elements forms gaseous oxides.

Powders that contain SE are often referred to as self-fluxing alloys since they were intended to produce dense coatings by having similar effects as fused coatings, although post-deposition fusing is sometimes still required. The SE used in such applications typically has a lower melting point and is more easily oxidized than the base material (BM). Self-fluxing alloys function by incorporating a thermally oxidizable element, such as aluminum, that

reacts exothermically with oxygen to release a large amount of heat to produce good bonding. For this reason, such powders are also used as a bond coat to improve adhesion of coating to metal substrates. These powders are either manufactured as (i) SE-coated particles with a metallic core or (ii) powder mixture or agglomerated particles containing SE. Examples of such powders are listed in Table 6. For powders manufactured in the form (ii), the SE particles are typically smaller than the particles of BM since this will provide the SE particles with greater surface area and hence greater tendency to oxidize in preference to the BM (Ref 108). The percentages of SE in the powders vary depending on the type of material and oxidation effects desired; refer to examples in Table 6.

## 6. Gaging the Effects of Oxidation via Hardness Testing

The extent of oxidation that occurred during processing can be measured by various techniques, such as image analysis (Ref 70, 109, 110) and analysis of the oxygen/

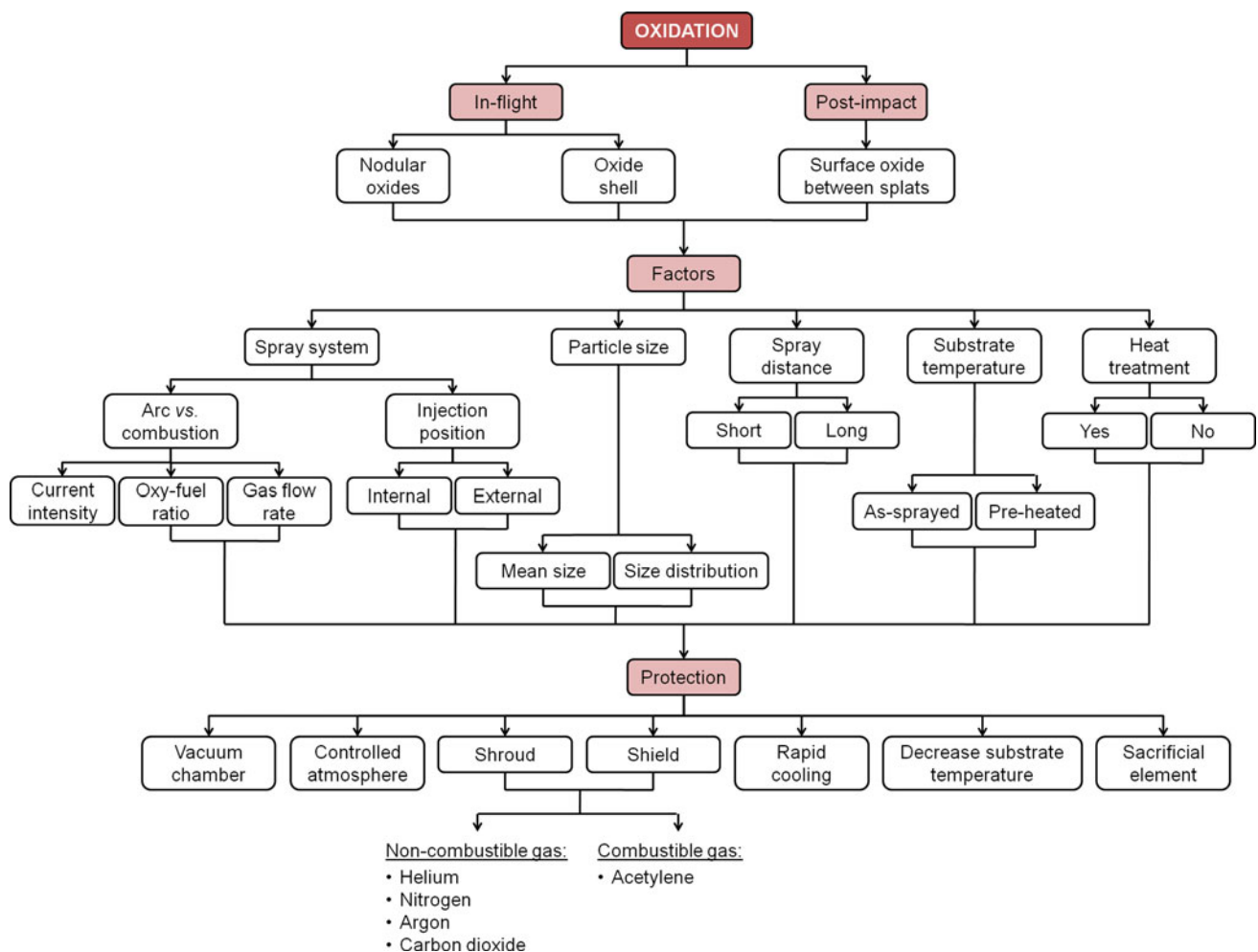


Fig. 17 Flowchart of oxidation considerations for thermal spray processing of materials

nitrogen content (Ref 59, 111). Hardness or indentation tests present a simple, indirect approach to measure the approximate oxide content in a material. The occurrence of oxidation is reflected in the hardness values of the coatings since metal oxides generally exhibit higher hardness compared to their metallic counterparts. A comparison of hardness values between metal and their oxides is presented in Table 7. Oxidation of Nd-Fe-B has also been evidenced to result in increased hardness (Ref 29).

Hardness of thermal sprayed coatings has been established to depend on the combined effects of unmelts, porosity, residual stresses, and oxide inclusions within the coatings. Although there have been no direct correlations established between hardness and oxide content, the coating hardness tends to increase with an increase in oxide content (Ref 59). Other work (Ref 101, 112) has also attributed the variation of hardness in thermal sprayed coatings to the presence of oxides. Therefore, hardness testing methods can provide an estimate of oxide content when a suitable calibration is carried out. Figure 16 shows an example of hardness value variations with oxygen content in a coating.

The practicality of using a hardness test or micro-indentation test to evaluate the effects of oxidation is demonstrated by its use in evaluating mechanical property changes and damage in TBCs induced by oxidation and residual stresses (Ref 113, 114). TBCs are applied to superalloy materials to reduce oxidation and thermal fatigue of load-bearing alloys for high temperature applications. TBCs consist of a ceramic top coat and a metallic bond coat that is applied to a superalloy substrate. A thermally grown oxide (TGO) layer, which results from oxidation of the bond coat, develops at the interface between the top coat and bond coat during thermal cycling. The TGO layer causes a thermal expansion mismatch and development of stresses, which result in coating spalling and failure.

However, the evaluation of oxidation behavior in TBCs is more complex than as-sprayed coatings where oxidation occurs during deposition, due to different oxidation mechanisms. Other factors, such as effects of sintering, oxide scale growth, and development of cracks, need to be taken into consideration since they have varying effects on the mechanical properties. Reviews on TBCs and their failure mechanisms are available in (Ref 115, 116).

## 7. Conclusions

Oxidation of thermal spray coatings poses concerns in applications in which the oxides interfere with the performance of the coatings, such as in corrosion resistance, magnetic properties, and mechanical properties. The mechanisms and influencing factors of oxidation must be understood in order to control the extent of their oxidation by implementing protection measures. The flow chart in Fig. 17 summarizes the oxidation considerations for thermal spray process and forms part of the

decision-making process in determining the appropriate spray parameters and protection measures to use for the desired oxidation effects.

Application of PMCs by thermal spray processes is still limited due to oxidation concerns. Oxidation causes the loss of ferromagnetic phases and leads to deterioration of magnetic properties. Oxidation of PMCs during the fabrication process is still not completely understood since most studies are centered on oxidation during aging. Thermal oxidation of neodymium iron boron and samarium cobalt occurs over two stages: (i) formation of external scales and (ii) internal oxidation. Neodymium iron boron undergoes dissociation followed by oxidation to form  $\alpha$ -Fe<sub>2</sub>O<sub>3</sub> and Fe<sub>3</sub>O<sub>3</sub> on its external scales and  $\alpha$ -Fe, Nd<sub>2</sub>O<sub>3</sub>, NdFeO<sub>3</sub>, and B<sub>2</sub>O<sub>3</sub> in its IOZ. On the other hand, the oxidation mechanism for samarium cobalt is still not fully understood. However, most oxidation studies agreed on the oxidation products of Co<sub>3</sub>O<sub>4</sub> and CoFe<sub>2</sub>O<sub>4</sub> on the external scales and  $\alpha$ -Co, Sm<sub>2</sub>O<sub>3</sub>, and SmCo<sub>3</sub> in its IOZ. Further work is still necessary to understand the oxidation of PMCs in thermal spray process.

There are two stages of oxidation in thermal spray coatings: (i) in-flight and (ii) post-impact oxidation. In-flight oxidation encompasses two regions: (i) the jet core and (ii) beyond the jet core and before impact onto the substrate, where local atmosphere is entrained into the flame. Post-impact oxidation refers to the deposition, solidification, and cooling stages. The majority of oxidation occurs at the in-flight stage due to the high temperature and oxygen entrainment, although the exposure to oxygen during post-impact is longer than the in-flight time. In-flight oxidation resulted in nodular oxides and oxide shells, while post-impact oxidation produces surface oxides between splat layers.

The factors that influence oxidation rely on the oxidation process that dominates, and this depends on the spray system, powder injection position, and particle size of the feedstock. In cases where in-flight oxidation is in control, the extent of oxidation is influenced by the oxygen-fuel ratio, current intensity, gas flow rate, particle size, and spray distance. Extent of oxidation is governed by the substrate temperature and spray distance when post-impact oxidation is dominant.

Considering the detrimental effects of oxidation for rare-earth magnetic materials, some extent of oxidation protection is possible for these materials to be deposited *via* the thermal spray process. The protection measure would depend on the oxidation process that is in dominance, i.e., in-flight or post-impact oxidation. Shrouding is considered the most effective as well as economical and practical protection method, where its principal is based on minimizing air entrainment. Shrouding should be employed where in-flight oxidation is in control, while shielding is more appropriate where post-impact oxidation dominates. Inert gases such as argon, nitrogen, and helium are typically used, although acetylene and carbon dioxide were also proven to be effective shrouding agents. The extent of air entrainment reduction depends on the mass and volume flow rate of the gases due to the differences in gas densities. SEs can also be used to minimize oxidation.

The oxidation protection measures used should be designed for a specific spray system to achieve the optimum effect since each system has unique geometrical needs. Consideration also needs to be turned to the geometry of the substrate since this will influence the gas flow fields during the spray process.

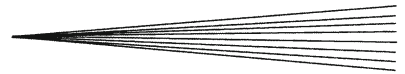
Finally, indentation tests present a viable, simple alternative in evaluating the effects of oxidation in thermal sprayed coatings. However, this approach needs to be used judiciously since hardness values depend not only on oxide inclusions but also on other microstructural artifacts such as unmelts and porosity.

## Acknowledgments

The authors would like to acknowledge the financial support by a Swinburne University Postgraduate Research Award (SUPRA) for this research and development of thermal spray processing of magnetic coatings.

## References

- M. Martena, D. Botto, P. Fino, S. Sabbadini, M.M. Gola, and C. Badini, Modelling of TBC System Failure: Stress Distribution as a Function of TGO Thickness and Thermal Expansion Mismatch, *Eng. Fail. Anal.*, 2006, **13**(3), p 409-426
- S. Deshpande, S. Sampath, and H. Zhang, Mechanisms of Oxidation and Its Role in Microstructural Evolution of Metallic Thermal Spray Coatings—Case Study for Ni-Al, *Surf. Coat. Technol.*, 2006, **200**(18-19), p 5395-5406
- S.E. Hartfield-Wünsch and S.C. Tung, The Effect of Microstructure on the Wear Behavior of Thermal Spray Coatings, *Thermal Spray Industrial Applications*, C.C. Berndt and S. Sampath, Ed., ASM International, Materials Park, 1994, p 19-24
- J. Alcalá, F. Gaudette, S. Suresh, and S. Sampath, Instrumented Spherical Micro-Indentation of Plasma-Sprayed Coatings, *Mater. Sci. Eng. A*, 2001, **316**(1-2), p 1-10
- K. Voleník, V. Novák, J. Dubský, P. Chráska, and K. Neufuss, Properties of Alloy Steel Coatings Oxidized During Plasma Spraying, *Mater. Sci. Eng. A*, 1997, **234-236**, p 493-496
- R. Goswami, H. Herman, S. Sampath, X. Jiang, Y. Tian, and G. Halada, Plasma Sprayed Mo-Mo Oxide Nanocomposites: Synthesis and Characterization, *Surf. Coat. Technol.*, 2001, **141**(2-3), p 220-226
- R. Harris and A.J. Williams, Attractions of Rare Earth Magnets, *Mater. World*, 1999, **7**(8), p 478-481
- T.S. Chin, Permanent Magnet Films for Applications in Microelectromechanical Systems, *J. Magn. Magn. Mater.*, 2000, **209**(1-3), p 75-79
- D.P. Arnold and N. Wang, Permanent Magnets for MEMS, *J. Microelectromech. Syst.*, 2009, **18**(6), p 1255-1266
- J.J. Wysocki, Magnetic Properties, Microstructures and Domain Structures of Arc-Plasma Sprayed Nd-Fe-B Permanent Magnet, *J. Mater. Sci.*, 1992, **27**(14), p 3777-3781
- G. Rieger, J. Wecker, W. Rodewald, W. Sattler, F.W. Bach, T. Duda, and W. Unterberg, Nd-Fe-B Permanent Magnets (Thick Films) Produced by a Vacuum-Plasma-Spraying Process, *J. Appl. Phys.*, 2000, **87**(9), p 5329-5331
- M. Willson, S. Bauser, S. Liu, and M. Huang, Plasma Sprayed Nd-Fe-B Permanent Magnets, *J. Appl. Phys.*, 2003, **93**(10), p 7987-7989
- P.C. King, S.H. Zahiri, and M.Z. Jahedi, Rare Earth/Metal Composite Formation by Cold Spray, *J. Therm. Spray Technol.*, 2008, **17**(2), p 221-227
- W.F. Liu, S. Suzuki, and K. Machida, Magnetic Properties of Nd-Fe-B Film Magnets Prepared by RF Sputtering, *J. Magn. Magn. Mater.*, 2007, **308**(1), p 126-130
- S.L. Chen, W. Liu, Z.D. Zhang, and G.H. Gunaratne, Magnetic Properties and Magnetic Domains of Nd-Fe-B Thin Films, *J. Appl. Phys.*, 2008, **103**(2), Article number 023922 (6 pp)
- B. Pawlowski and J. Töpfer, Permanent Magnetic NdFeB Thick Films, *J. Mater. Sci.*, 2004, **39**(4), p 1321-1324
- T. Speliotis, D. Niarchos, P. Falaras, D. Tsoukleris, and J. Pepin, Nd-Fe-B Thick Films Prepared by Screen Printing, *IEEE Trans. Magn.*, 2005, **41**(10), p 3901-3903
- B. Pawlowski, H. Beer, and J. Toepfer, Preparation of Nd-Fe-B Magnetic Films by Ceramic Techniques, *Key Eng. Mater.*, 1997, **132-136**(Part 2), p 1409-1411
- B. Pawlowski, S. Schwarzer, A. Rahmig, and J. Töpfer, NdFeB Thick Films Prepared by Tape Casting, *J. Magn. Magn. Mater.*, 2003, **265**(3), p 337-344
- R.A. Overfelt, C.D. Anderson, and W.F. Flanagan, Plasma Sprayed Fe<sub>76</sub>Nd<sub>16</sub>B<sub>8</sub> Permanent Magnets, *Appl. Phys. Lett.*, 1986, **49**(26), p 1799-1801
- J. Jacobson and A. Kim, Oxidation Behavior of Nd-Fe-B Magnets, *J. Appl. Phys.*, 1987, **61**(8), p 3763-3765
- A.S. Kim and J. Jacobson, Oxidation and Oxidation Protection of Nd-Fe-B Magnets, *IEEE Trans. Magn.*, 1987, **MAG-23**(5), p 2509-2511
- P. Tenaud, F. Vial, and M. Sagawa, Improved Corrosion and Temperature Behaviour of Modified Nd-Fe-B Magnets, *IEEE Trans. Magn.*, 1990, **26**(5), p 1930-1932
- K. Tokuhara and S. Hirosawa, Corrosion Resistance of Nd-Fe-B Sintered Magnets, *J. Appl. Phys.*, 1991, **69**(8), p 5521-5523
- F.E. Camp and A.S. Kim, Effect of Microstructure on the Corrosion Behavior of NdFeB and NdFeCoAlB Magnets, *J. Appl. Phys.*, 1991, **70**(10), p 6348-6350
- T.S. Chin, R.T. Chang, W.T. Tsai, and M.P. Hung, Electrochemical Behavior of Rare-Earth Magnet Alloys in Various Solutions, *IEEE Trans. Magn.*, 1987, **24**(2), p 1927-1929
- H. Bala, S. Szymura, and J.J. Wysocki, Electrochemical Corrosion Resistance of Fe-Nd-B Permanent Magnets, *J. Mater. Sci.*, 1990, **25**(1), p 571-574
- G.W. Warren, G. Gao, and Q. Li, Corrosion of NdFeB Permanent Magnet Materials, *J. Appl. Phys.*, 1991, **70**(10), p 6609-6611
- J.-M. Le Breton, J. Teillet, P.J. McGuinness, D.S. Edgley, and R. Harris, The Oxidation of a Nd-Fe-B Permanent Magnet at 400°C: A SEM, Microhardness and Mössbauer Study, *IEEE Trans. Magn.*, 1992, **28**(5), p 2157-2159
- D.S. Edgley, J.M. Le Breton, D. Lemarchand, I.R. Harris, and J. Teillet, Dissociation of Nd<sub>2</sub>Fe<sub>14</sub>B During High Temperature Oxidation, *J. Magn. Magn. Mater.*, 1993, **128**(1-2), p L1-L7
- P. Fauchais, A. Vardelle, and B. Dussoubs, Quo Vadis Thermal Spraying?, *J. Therm. Spray Technol.*, 2001, **10**(1), p 44-66
- P. Fauchais, Understanding Plasma Spraying, *J. Phys. D: Appl. Phys.*, 2004, **37**(9), p R86-R108
- J.A. Gan and C.C. Berndt, Design and Manufacture of Nd-Fe-B Thick Coatings by the Thermal Spray Process, *Surf. Coat. Technol.*, 2011, **205**(19), p 4697-4704
- J.A. Gan and C.C. Berndt, Effects of Standoff Distance on Porosity, Phase Distribution and Mechanical Properties of Plasma Sprayed Nd-Fe-B Coatings, *Surf. Coat. Technol.*, 2013, **216**, p 127-138
- V. De Pauw, D. Lemarchand, and J.J. Malandain, A Structural and Kinetic Study of the Oxidation of the Intermetallic Sm<sub>2</sub>(Fe, Co)<sub>17</sub> Compound for Permanent Magnets, *J. Magn. Magn. Mater.*, 1997, **172**(3), p 269-276
- Y. Li, H.E. Evans, I.R. Harris, and I.P. Jones, The Oxidation of NdFeB Magnets, *Oxid. Met.*, 2003, **59**(1-2), p 167-182
- W.M. Pragnell, A.J. Williams, and H.E. Evans, The Oxidation of SmCo Magnets, *J. Appl. Phys.*, 2008, **103**(7), Article number 07E127 (3 pp)
- S. Kardelky, A. Gebert, O. Gutfleisch, A. Handstein, U. Wyss, and L. Schultz, Corrosion Behavior of Sm-Co-Based Permanent Magnets in Oxidizing Environments, *IEEE Trans. Magn.*, 2004, **40**(4), p 2931-2933



39. Z. Yang, X. Peng, Q. Feng, Z. Guo, W. Li, and F. Wang, The Mechanism of High Temperature Oxidation of a SmCo-Based Magnetic Alloy, *Corros. Sci.*, 2012, **61**, p 72-82
40. D.S. Edgley, J.M. Le Breton, S. Steyaert, F.M. Ahmed, I.R. Harris, and J. Teillet, Characterisation of High Temperature Oxidation of Nd-Fe-B Magnets, *J. Magn. Magn. Mater.*, 1997, **173**(1-2), p 29-42
41. R.W. Bartlett and P.J. Jorgensen, Microstructure and Growth Kinetics of the Fibrous Composite Subscale Formed by Internal Oxidation of SmCo<sub>5</sub>, *Metall. Trans.*, 1974, **5**(2), p 355-361
42. J.M. Le Breton and J. Teillet, Oxidation of (Nd, Dy)FeB Permanent Magnets Investigated by <sup>57</sup>Fe Mossbauer Spectroscopy, *IEEE Trans. Magn.*, 1990, **26**(5), p 2652-2654
43. L. Castaldi, M.R.J. Gibbs, and H.A. Davies, Effect of the Substrate Temperature on the Properties of RE-Fe-B Thin Film Magnets, *J. Appl. Phys.*, 2004, **96**(9), p 5063-5068
44. M. Nakano, S. Sato, F. Yamashita, T. Honda, J. Yamasaki, K. Ishiyama, M. Itakura, J. Fidler, T. Yanai, and H. Fukunaga, Review of Fabrication and Characterization of Nd-Fe-B Thick Films for Magnetic Micromachines, *IEEE Trans. Magn.*, 2007, **43**(6), p 2672-2676
45. A.S. Lileev, A.A. Parilov, and V.G. Blatov, Properties of Hard Magnetic Nd-Fe-B Films Versus Different Sputtering Conditions, *J. Magn. Magn. Mater.*, 2002, **242-245**(Part 2), p 1300-1303
46. S.L. Chen, J.G. Zheng, W. Liu, and Z.D. Zhang, Structure and Magnetic Properties of High-Energy Product Nd-Fe-B/Nd-O Thin Films, *J. Phys. D: Appl. Phys.*, 2007, **40**(6), p 1816-1820
47. W. Rodewald, Rare-Earth Transition-Metal Magnets, *Handbook of Magnetism and Advanced Magnetic Materials*, H. Kronmüller and S. Parkin, Ed., Wiley, New York, 2007,
48. M.I. Qadeer, B. Azhdar, M.S. Hedenqvist, and S.J. Savage, Anomalous High Temperature Oxidation of Sm<sub>2</sub>(Fe, Co., Cu, Zr)<sub>17</sub> Particles, *Corros. Sci.*, 2012, **65**, p 453-460
49. V. De Pauw, D. Lemarchand, J.M. Saiter, and C. Devallencourt, Oxidation Study of Bulk and Powdered Sm<sub>2</sub>(Fe<sub>0.5</sub>Co<sub>0.5</sub>)<sub>17</sub>N<sub>x</sub> (x = 0, 2.9) Compounds, *J. Alloys Compd.*, 1998, **266**(1-2), p 293-299
50. W.M. Pragnell, H.E. Evans, and A.J. Williams, Oxidation Protection of Sm<sub>2</sub>Co<sub>17</sub>-Based Alloys, *J. Alloys Compd.*, 2012, **517**, p 92-97
51. N. Asahi, K. Asaka, K. Ueda, and M. Sasaki, Thermal Spray of Nd-Fe-B, *First International Conference on Processing Materials for Properties*, H. Henein and T. Oki, Ed., The Minerals, Metals & Materials Society (TMS), Warrendale, 1993, p 1197-1200
52. K. Turek, P. Liszkowski, and H. Figiel, Kinetics of Oxidation of Nd-Fe-B Powders, *IEEE Trans. Magn.*, 1993, **29**(6), p 2782-2784
53. K.J. Strnat and R.M.W. Strnat, Rare Earth-Cobalt Permanent Magnets, *J. Magn. Magn. Mater.*, 1991, **100**(1-3), p 38-56
54. E. Burzo, Permanent Magnets Based on R-Fe-B and R-Fe-C Alloys, *Rep. Prog. Phys.*, 1998, **61**(11), p 1099-1266
55. M. Matsuura, R. Goto, N. Tezuka, and S. Sugimoto, Influence of Nd Oxide Phase on the Coercivity of Nd-Fe-B Thin Films, *Mater. Trans.*, 2010, **51**(10), p 1901-1904
56. S. Heisz and G. Hilscher, The Origin of Graduated Demagnetization Curves of NdFeB Magnets, *J. Magn. Magn. Mater.*, 1987, **67**(1), p 20-28
57. E.D. Dickens, Jr, and A.M. Mazany, The Corrosion and Oxidation of Nd-Fe-B Magnets, *J. Appl. Phys.*, 1990, **67**(9), p 4613-4615
58. C.M. Hackett and G.S. Settles, Research on HVOF Gas Shrouding for Coating Oxidation Control, *Advances in Thermal Spray Science & Technology*, C.C. Berndt and S. Sampath, Ed., ASM International, Materials Park, 1995, p 21-29
59. K. Dobler, H. Kreye, and R. Schwetke, Oxidation of Stainless Steel in the High Velocity Oxy-Fuel Process, *J. Therm. Spray Technol.*, 2000, **9**(3), p 407-413
60. M. Li and P.D. Christofides, Computational Study of Particle In-Flight Behavior in the HVOF Thermal Spray Process, *Chem. Eng. Sci.*, 2006, **61**(19), p 6540-6552
61. A. Vardelle, P. Fauchais, and N.J. Themelis, Oxidation of Metal Droplets in Plasma Sprays, *Advances in Thermal Spray Science & Technology*, C.C. Berndt and S. Sampath, Ed., ASM International, Materials Park, 1995, p 175-180
62. H. Zhang, A. Vardelle, and N.J. Themelis, In-Flight Oxidation and Evaporation of Plasma-Sprayed Iron Particles, *J. High Temp. Mater. Process.*, 2003, **7**(3), p 277-298
63. K. Voleník, F. Hanousek, P. Chráska, J. Ilavský, and K. Neufuss, In-Flight Oxidation of High-Alloy Steels During Plasma Spraying, *Mater. Sci. Eng.*, 1999, **272**(1), p 199-206
64. A.A. Syed, A. Denoirjean, P. Denoirjean, J.C. Labbe, and P. Fauchais, Influence of Plasma Spraying Parameters on the In-Flight Oxidation of Stainless Steel Particles, *Thermal Spray 2004: Advances in Technology and Application*, ASM International, Materials Park, 2004, p. 277-282
65. A.A. Syed, A. Denoirjean, P. Fauchais, and J.C. Labbe, On the Oxidation of Stainless Steel Particles in the Plasma Jet, *Surf. Coat. Technol.*, 2006, **200**(14-15), p 4368-4382
66. V.V. Sobolev and J.M. Guilemany, Effect of Oxidation on Droplet Flattening and Splat-Substrate Interaction in Thermal Spraying, *J. Therm. Spray Technol.*, 1999, **8**(4), p 523-530
67. H. Ageorges and P. Fauchais, Oxidation of Stainless Steel Particles With and Without an Alumina Shell During Their Flight in a Plasma Jet, *High Temp. Mater. Process.*, 2000, **4**(3), p 323-337
68. R.A. Neiser, M.F. Smith, and R.C. Dykhuizen, Oxidation in Wire HVOF-Sprayed Steel, *J. Therm. Spray Technol.*, 1998, **7**(4), p 537-545
69. G. Espie, A. Denoirjean, P. Fauchais, J.C. Labbe, J. Dubsky, O. Schneeweiss, and K. Volenik, In-Flight Oxidation of Iron Particles Sprayed Using Gas and Water Stabilized Plasma Torch, *Surf. Coat. Technol.*, 2005, **195**(1), p 17-28
70. A.A. Syed, A. Denoirjean, P. Denoirjean, J.C. Labbe, and P. Fauchais, In-Flight Oxidation of Stainless Steel Particles in Plasma Spraying, *J. Therm. Spray Technol.*, 2005, **14**(1), p 117-124
71. M.J.M. Hill, On a Spherical Vortex, *Phil. Trans. R. Soc. Lond. A*, 1894, **185**, p 213-245
72. V.V. Sobolev and J.M. Guilemany, Oxidation of Coatings in Thermal Spraying, *Mater. Lett.*, 1998, **37**(4-5), p 231-235
73. C.J. Li and W.Y. Li, Effect of Sprayed Powder Particle Size on the Oxidation Behavior of MCrAlY Materials During High Velocity Oxygen-Fuel Deposition, *Surf. Coat. Technol.*, 2003, **162**(1), p 31-41
74. A. Vardelle, M. Vardelle, H. Zhang, N.J. Themelis, and K. Gross, Volatilization of Metal Powders in Plasma Sprays, *J. Therm. Spray Technol.*, 2002, **11**(2), p 244-252
75. C.M. Hackett and G.S. Settles, Turbulent Mixing of the HVOF Thermal Spray and Coating Oxidation, *Thermal Spray Industrial Applications*, C.C. Berndt and S. Sampath, Ed., ASM International, Materials Park, 1994, p 307-312
76. S. Matthews, B. James, and M. Hyland, The Effect of Heat Treatment on the Oxidation Mechanism of Blended Powder Cr<sub>3</sub>C<sub>2</sub>-NiCr Coatings, *J. Therm. Spray Technol.*, 2010, **19**(1-2), p 119-127
77. Z. Zeng, S. Kuroda, J. Kawakita, M. Komatsu, and H. Era, Effects of Some Light Alloying Elements on the Oxidation Behavior of Fe and Ni-Cr Based Alloys During Air Plasma Spraying, *J. Therm. Spray Technol.*, 2010, **19**(1-2), p 128-136
78. T. Fukushima and S. Kuroda, Oxidation of HVOF Sprayed Alloy Coatings and Its Control by a Gas Shroud, *Thermal Spray 2001: New Surfaces for a New Millennium*, C.C. Berndt, K.A. Khor, and E.F. Lugscheider, Ed., ASM International, Materials Park, 2001, p 527-532
79. R. Knight and R.W. Smith, HVOF Sprayed 80/20 NiCr Coatings-Process Influence Trends, *Thermal Spray: International Advances in Coatings Technology*, C.C. Berndt, Ed., ASM International, Materials Park, 1992, p 159-164
80. H. Voggenreiter, H. Huber, S. Beyer, and H.J. Spies, Influence of Particle Velocity and Molten Phase on the Chemical and Mechanical Properties of HVOF-Sprayed Structural Coatings of Alloy 316L, *Advances in Thermal Spray Science & Technology*, C.C. Berndt and S. Sampath, Ed., ASM International, Materials Park, 1995, p 303-308
81. L.N. Moskowitz, and D.J. Lindley, High Density Thermal Spray Coating, U.S. Patent 5,151,308, Amoco Corporation (Chicago, IL) issued 29 Sept. 1992
82. J. Kim, K. Kang, S. Yoon, S. Kumar, H. Na, and C. Lee, Oxidation and Crystallization Mechanisms in Plasma-Sprayed Cu-Based Bulk Metallic Glass Coatings, *Acta Mater.*, 2010, **58**(3), p 952-962

83. D. Cheng, Q. Xu, G. Trapaga, and E.J. Lavernia, A Numerical Study of High-Velocity Oxygen Fuel Thermal Spraying Process. Part I: Gas Phase Dynamics, *Metall. Mater. Trans. A*, 2001, **32**(7), p 1609-1620
84. W. Zhang, L.L. Zheng, H. Zhang, and S. Sampath, Study of Injection Angle and Carrier Gas Flow Rate Effects on Particles In-Flight Characteristics in Plasma Spray Process: Modeling and Experiments, *Plasma Chem. Plasma Process.*, 2007, **27**(6), p 701-716
85. M.P. Planche, H. Liao, and C. Coddet, Oxidation Control in Atmospheric Plasma Spraying Coating, *Surf. Coat. Technol.*, 2007, **202**(1), p 69-76
86. O. Kovářík, X. Fan, and M. Boulos, In Flight Properties of W Particles in an Ar-H<sub>2</sub> Plasma, *J. Therm. Spray Technol.*, 2007, **16**(2), p 229-237
87. V. Gourlaouen, E. Verna, and P. Beaubien, Influence of Flame Parameters on Stainless Steel Coatings Properties, *Thermal Spray: Surface Engineering via Applied Research*, C.C. Berndt, Ed., ASM International, Materials Park, 2000, p 487-493
88. V. Gourlaouen, E. Verna, K. Khor, and P.S.T. Guek, Role of Some Fuel Gases on Properties of HVOF Metallic Coatings, *Thermal Spray 2001: New Surfaces for a New Millennium*, C.C. Berndt, Ed., ASM International, Materials Park, 2001, p 519-525
89. D. Seo, K. Ogawa, T. Shoji, and S. Murata, Effect of Particle Size Distribution on Isothermal Oxidation Characteristics of Plasma Sprayed CoNi- and CoCrAlY Coatings, *J. Therm. Spray Technol.*, 2007, **16**(5-6), p 954-966
90. C.J. Li, H.T. Wang, Q. Zhang, G.J. Yang, W.Y. Li, and H. Liao, Influence of Spray Materials and Their Surface Oxidation on the Critical Velocity in Cold Spraying, *J. Therm. Spray Technol.*, 2010, **19**(1-2), p 95-101
91. G. Espie, P. Fauchais, J.C. Labbe, A. Vardelle, and B. Hannoyer, Oxidation of Iron Particles During APS: Effect of the Process on Formed Oxide Wetting of Droplets on Ceramics Substrates, *Thermal Spray 2001: New Surfaces for a New Millennium*, C.C. Berndt, K.A. Khor, and E.F. Laguscheider, Ed., ASM International, Materials Park, 2001, p 821-827
92. S.H. Zahiri, D. Fraser, S. Gulizia, and M. Jahedi, Effect of Processing Conditions on Porosity Formation in Cold Gas Dynamic Spraying of Copper, *J. Therm. Spray Technol.*, 2006, **15**(3), p 422-430
93. Z. Zeng, N. Sakoda, T. Tajiri, and S. Kuroda, Structure and Corrosion Behavior of 316L Stainless Steel Coatings Formed by HVOF Spraying With and Without Sealing, *Surf. Coat. Technol.*, 2008, **203**(1-2), p 284-290
94. J.E. Jackson, Method for Shielding a Gas Effluent, U.S. Patent 3,470,347, Union Carbide Corporation (New York, NY), issued 30 Sept. 1969
95. A.J. Rotolico, and J.R. Weodarczy, Shrouded Thermal Spray Gun and Method, U.S. Patent 4,964,568, The Perkin-Elmer Corporation (Norwalk, CT), issued 23 Oct. 1990
96. W. Simm, H.-T. Steine, and K.P. Streb, Apparatus for the Flame Spraying of Powder Materials by Means of an Autogenous Flame, U.S. Patent 5,014,915, Castolin S.A. (St. Sulpice, CH) issued 14 May 1991
97. C. Reiter, Device for the Production of a Protective Gas Mantle in Plasma Spraying, U.S. Patent 5,154,354, Nova-Werke AG (Effretikon, CH), issued 13 Oct. 1992
98. A. Dolatabadi, J. Mostaghimi, and V. Pershin, Effect of a Cylindrical Shroud on Particle Conditions in High Velocity Oxy-Fuel Spray Process, *Sci. Technol. Adv. Mater.*, 2002, **3**(3), p 245-255
99. I. Thomson, V. Pershin, J. Mostaghimi, and S. Chandra, Experimental Testing of a Curvilinear Gas Shroud Nozzle for Improved Plasma Spraying, *Plasma Chem. Plasma Process.*, 2001, **21**(1), p 65-82
100. M. Jankovic, J. Mostaghimi, and V. Pershin, Design of a New Nozzle for Direct Current Plasma Guns with Improved Spraying Parameters, *J. Therm. Spray Technol.*, 2000, **9**(1), p 114-120
101. X. Wang, J. Heberlein, E. Pfender, and W. Gerberich, Effect of Nozzle Configuration, Gas Pressure, and Gas Type on Coating Properties in Wire Arc Spray, *J. Therm. Spray Technol.*, 1999, **8**(4), p 565-575
102. X. Wang, Effect of Shrouded CO<sub>2</sub> Gas Atomization on Coating Properties in Wire Arc Spray, *Advances in Thermal Spray Science & Technology*, C.C. Berndt and S. Sampath, Ed., ASM International, Materials Park, 1995, p 31-37
103. K.D. Kang and S.H. Hong, Numerical Analysis of Shroud Gas Effects on Air Entrainment into Thermal Plasma Jet in Ambient Atmosphere of Normal Pressure, *J. Appl. Phys.*, 1999, **85**(9), p 6373-6380
104. D.T. Gawne, T. Zhang, and B. Liu, Computational Analysis of the Influence of a Substrate, Solid Shield and Gas Shroud on the Flow Field of a Plasma Jet, *Surf. Coat. Technol.*, 2002, **153**(2-3), p 138-147
105. S. Jamais, M. Creaven, and C. Rinaldi, Calculated and Measured Oxygen Contents in the Gas Flow of a Shrouded Thermal Spray Process, *Thermal Spray 2001: New Surfaces for a New Millennium*, C.C. Berndt, K.A. Khor, and E.F. Laguscheider, Ed., ASM International, Materials Park, 2001, p 903-910
106. K. Cheng, X. Chen, H.X. Wang, and W. Pan, Modeling Study of Shrouding Gas Effects on a Laminar Argon Plasma Jet Impinging upon a Flat Substrate in Air Surroundings, *Thin Solid Films*, 2006, **506-507**, p 724-728
107. Z. Zeng, S. Kuroda, and H. Era, Comparison of Oxidation Behavior of Ni-20Cr Alloy and Ni-Base Self-Fluxing Alloy During Air Plasma Spraying, *Surf. Coat. Technol.*, 2009, **204**(1-2), p 69-77
108. M.S. Patel, Flame Spray Powder Mix, U.S. Patent 4,230,748, Eutectic Corporation (Flushing, NY), issued 28 Oct. 1980
109. V. Higuera, F.J. Belzunce, A. Carriles, and S. Poveda, Influence of the Thermal-Spray Procedure on the Properties of a Nickel-Chromium Coating, *J. Mater. Sci.*, 2002, **37**(3), p 649-654
110. M.P. Planche, H. Liao, B. Normand, and C. Coddet, Relationships Between NiCrBSi Particle Characteristics and Corresponding Coating Properties Using Different Thermal Spraying Processes, *Surf. Coat. Technol.*, 2005, **200**(7), p 2465-2473
111. Q. Wei, Z. Yin, and H. Li, Oxidation Control in Plasma Spraying NiCrCoAlY Coating, *Appl. Surf. Sci.*, 2012, **258**(12), p 5094-5099
112. R.A. Mahesh, R. Jayaganthan, and S. Prakash, Oxidation Behavior of HVOF Sprayed Ni-5Al Coatings Deposited on Ni- and Fe-Based Superalloys Under Cyclic Condition, *Mater. Sci. Eng. A*, 2008, **475**(1-2), p 327-335
113. J.P. Singh, B.G. Nair, D.P. Renuch, M.P. Sutarra, and M.H. Grimsditch, Damage Evolution and Stress Analysis in Zirconia Thermal Barrier Coatings During Cyclic and Isothermal Oxidation, *J. Am. Ceram. Soc.*, 2001, **84**(10), p 2385-2393
114. M. Eskner and R. Sandström, Mechanical Properties and Temperature Dependence of an Air Plasma-Sprayed NiCoCrAlY Bondcoat, *Surf. Coat. Technol.*, 2006, **200**(8), p 2695-2703
115. A.G. Evans, D.R. Mumm, J.W. Hutchinson, G.H. Meier, and F.S. Pettit, Mechanisms Controlling the Durability of Thermal Barrier Coatings, *Prog. Mater. Sci.*, 2001, **46**(5), p 505-553
116. D.R. Clarke and C.G. Levi, Materials Design for the Next Generation Thermal Barrier Coatings, *Annu. Rev. Mater. Res.*, 2003, **33**, p 383-417
117. C. Tekmen, Y. Tsunekawa, M. Yoshida, and M. Okumiya, Microstructural Characterization of In-Flight Particles in Plasma Spray Process, *Plasma Process. Polym.*, 2009, **6**(SUP-PL. 1), p S223-S226
118. N. Sakakibara, Y. Manabe, Y. Hiromoto, and Y. Kobayashi, Development of High Quality Thermal Sprayed Metal Coating Process by Shielding Control, *Thermal Spray 2004: Advances in Technology and Application*, 2004, p 595-599
119. J.E. Cromwell, Flame-Sprayable Composition of Nickel Coated Molybdenum, U.S. Patent 3,843,334, Koppers Company Inc., issued 22 Oct 1974
120. E.R. Novinski, and J.H. Harrington, Aluminium- and Molybdenum-Coated Nickel, Copper or Iron Core Flame Spray Materials, U.S. Patent 3,841,901, Metco Inc. (Westbury, NY), issued 15 Oct 1974
121. J.H. Harrington, and F.N. Longo, Composite Iron Molybdenum Boron Flame Spray Power, U.S. Patent 3,991,240, Metco Inc. (Westbury, NY), issued 9 Nov 1976



122. F.J. Dittrich, G.J. Durmann, and H.S. Ingham, Jr., Aluminium-Coated Nickel or Cobalt Core Flame Spray Materials, U.S. Patent 4,019,875, Metco Inc. (Westbury, NY), issued 26 Apr 26
123. J.H. Harrington, and S. Rangaswamy, Aluminium and Cobalt Coated Thermal Spray Powder, U.S. Patent 4,578,115, Metco Inc. (Westbury, NY), issued 25 Mar. 1986
124. S. Rangaswamy, and J.H. Harrington, Aluminium and Yttrium Oxide Coated Thermal Spray Powder, U.S. Patent 4,578,114, Metco Inc. (Westbury, NY), issued 25 Mar. 1986
125. S. Rangaswamy, and R.A. Miller, Composite Powders for Thermal Spray Coating, U.S. Patent 5,385,789, Sulzer Plasma Technik Inc. (Troy, MI), issued 31 Jan. 1995
126. F.J. Hermanek, Self-Bonding MCrAlY Powder, U.S. Patent 6,410,159 B1, Praxair S. T. Technology Inc. (North Haven, CT), issued 25 Jun. 2002
127. F.N. Longo, High Temperature Flame Spray Powder, U.S. Patent 3,313,633, Metco Inc. (Westbury, NY), issued 11 Apr. 1967
128. L. Russo, M.R. Dorfman, and K. LaPierre, 2002, Superalloy HVOF Powders with Improved High Temperature Oxidation, Corrosion and Creep Resistance, U.S. Patent 6,346,134 B1, Sulzer Metco Inc. (Westbury, NY), issued 12 Feb. 2002
129. R.W. Wilson, The Contact Resistance and Mechanical Properties of Surface Films on Metals, *Proc. Phys. Soc. B*, 1955, **68**(9), p 625-641